Characterization of the Role of Necroptosis for Oncolytic Vaccinia Efficacy

by

Aradhana Kasimsetty

A Thesis Presented in Partial Fulfillment
of the Requirements for the Degree
Master of Science

Approved April 2020 by the
Graduate Supervisory Committee:

Bertram Jacobs, Chair
Douglas McFadden
Mitesh Borad

ARIZONA STATE UNIVERSITY

May 2020

ABSTRACT

Since the molecular biology revolution in the 1980s, ease of gene editing had led to the resurgence of Oncolytic Virotherapy. Countless viruses have been engineered yet only three are approved for clinical use worldwide, with only one being approved by the U.S Food and Drug Administration (FDA). Vaccinia virus (VACV) has a large genome, contains many immune evasion genes and has been thoroughly studied, making it a popular candidate for an oncolytic platform. VACV mutants with deletions in the E3 immune evasion protein have been shown to have oncolytic efficacy but the mechanism of tumor selectivity has not been fully elucidated. These mutants have been shown to be regulated by the necroptosis pathway, a pathway that has been shown to be deficient in certain cancers. Using a pan-cancer screening method that combines dye exclusion assays, western blot analysis, and viral growth curve, the role of necroptosis in regulating VACV replication and oncolytic efficacy in cancer was further characterized. Results demonstrate a preliminary correlation between necroptosis, viral replication, and oncolytic efficacy. This correlation is clearest in breast cancer and melanomas yet may apply to other cancer subgroups. This data was also used to guide the development of a receptor-interacting protein kinase 3 (RIP3) matched pair mouse model in the E0771 mouse breast cancer line which can be used to further study the role of necroptosis and oncolytic efficacy in vivo. Understanding the contribution necroptosis plays in oncolytic efficacy can guide to design enhance the design of clinical trials to test VACV E3L mutants and may lead to better efficacy in humans and an improvement in clinical oncology.

ACKNOWLEDGMENTS

I would like to acknowledge the people who have supported me throughout my collegiate journey. Thank you to my family: my parents, and my sister, for supporting me financially and emotionally through my bachelor's and master's at ASU. Without your love and support, I never would have been able to dedicate myself to my work nor grow as a scholar as much as I was able to. I would like to thank all of my advisors, professors, and peers in the School of Life Sciences undergraduate and graduate office for all of your help along the way. Specifically, I would like to thank Ivy Esquibel for guiding me on the right path and encouraging me to pursue the 4+1 accelerated program. I would like to thank everyone involved in the SOLUR program, specifically Dr. Shelley Haydel and Dr. Jason Maarsingh. You helped me develop as a research scientist and taught me how to think critically about the way we communicate our thoughts. In addition, thank you, Dr. Haydel, for your countless, stunning recommendations that allowed me to continue pursuing opportunities outside of ASU during my bachelor's and master's. I also want to thank the SOLUR program's donors for allowing me to be supported financially for the undergraduate portion of my thesis.

There are many members of the Jacobs lab I need to thank. I am eternally grateful to my PI, Dr. Bertram Jacobs, for taking me into the lab as a freshman and providing the right mentorship that allowed me to fall in love with virology. My second largest thank you goes to my former post-doc mentor Dr. Latha Kannan. You trained me from the ground-up as a scientist, you were patient through all my stumbles and never stopped pushing me to dream bigger. You were also invaluable in helping me develop a connection with Dr. Borad and the Mayo Clinic system and I can't imagine where I

would be without you. I would like to thank Sambhavi Subramanian. We worked on the entire oncolytic virotherapy project side by side and there is no way this project would be where it is now without you. Thank you to Dr. Jeffrey Langland for supporting me financially for a year and allowing me to hone my western blot skills and helping me discover my love of viro-oncology. I also want to thank Samantha Cotsmire, James Bonner and Mateusz Scerba for patiently answering my countless questions and giving me invaluable advice on experimental design. Thank you to Megan McCaughan for teaching me immunofluorescence and engaging in great late-night conversations. Lastly, thank you to Wesley Hoyland for being a great undergraduate friend and lab partner. I love everyone in this lab, and I will sorely miss this amazing work environment.

I would also like to thank everyone on my committee, Dr. Jacobs, Dr. Grant McFadden, and Dr. Mitesh Borad for the time and contribution they have given to my project and my own career development. Thank you also to the members of Dr. McFadden's lab for providing assistance with the CRISPR-Cas9 portion of the project and providing some plasmid. Thank you to the members of Dr. Joesph Blattman's lab, specifically Kavita Manhas, for providing the K7M2-luc cells.

I would like to thank ASU Women in Philanthropy, School of Life Sciences Undergraduate Research Program (SOLUR), The Biodesign Institute and The Graduate Student Professional Association (GPSA) for their financial support of my project and scientific development. Thank you to all for believing in my potential and contributing to my success.

TABLE OF CONTENTS

Page

LIST OF TABLES

LIST OF FIGURES

CHAPTER 1

INTRODUCTION

While they have been studied for over 100 years, oncolytic virotherapy (OV) has reached a new height of popularity, especially with the first FDA approval of an oncolytic virus in 2015 (1). However, despite the initial success, the fact that the scientific community has developed only one FDA approved therapeutic indicates that there is a lot of work left to do in the OV field. Additionally, the current treatment is only approved for melanoma, which leaves a dearth of other cancer subtypes to target. Therefore, this study aims to add to the body of knowledge by characterizing a novel oncolytic virus strategy.

The underlying concept of oncolytic virotherapy can be understood as the similarities between the 2011 'Hallmarks of Cancer' established by Hanahan and Weinberg and the analogous hallmarks of virally infected cells (2). While the pathways such as immune evasion, replication and resisting cell death are different in both virally infection and cancer, the fact still remains that these characteristics are important for both phenomena. These 'hallmarks' or driver mutations that help tumors develop are also indications of a cell adapted to allow infection. A virus that is dependent on these defects to be able to replicate becomes replication restricted to tumor cells, allowing for a tumor selective virus.

1.1 History of Oncolytic Virotherapy (1800's-1990)

Both fields of oncology and virology evolved rapidly over the 20th century. Oncology evolved from only surgical excision of tumors to a field dominated by the three tenants: cut, burn, or poison aka surgery, radiotherapy or chemotherapy. On the other

hand, virology made its mark on the clinical world in the 20th century with the discovery of the first human virus in 1901 (3).

Although it took until the latter half of the century for researchers to develop standard methods for studying, measuring and visualizing these “contagious fluids” and discovering how viruses and tumors were intertwined, evidence of the oncolytic ability of viruses occurred even as early as the 1800s. In multiple cases, doctors began to notice that the co-occurrence of pathogenic diseases (indicated by an enlarged spleen) resulted in the regression of various leukemias (4, 5). These remissions were often temporary and ended with the patient dying from cancer-related complications.

In 1949, researchers observed that virally caused hepatitis caused Hodgkin’s lymphoma’s patients to go into remission and decided to deliberately deliver the hepatitis serum to 21 more lymphoma patients. Of those 21 cases, 13 contracted hepatitis and 7 saw improvement marking this study as one of the first clinical trials for oncolytic virotherapy (6). This was followed by many trials testing various naturally occurring viruses, including Epstein-Barr and various flaviviruses. However, flaviviruses like West Nile virus also increased the risk of neurotoxicity, leading to safety concerns (7). Other viruses such as adenoviruses, picornaviruses, poxviruses, and vesiculoviruses became popular, but ultimately lacked a good balance of safety and efficacy leading to a decline in the field in the 1970s and 1980s.

Researchers initially attempted to circumvent these issues by turning to non-human viruses. However, it was the era of genetic engineering and reverse genetics in virology which allowed oncolytic virotherapy to flourish.

1.2 Current Oncolytic Landscape (1990-Present)

While the original approach for oncolytic viruses was to test various wild-type viruses, the field shifted to focus on engineering viruses to improve safety and specificity. The first engineered oncolytic virus was developed in 1991. This virus was a mutant Herpes-Simplex Virus 1 (HSV-1) with a deletion in the thymidine kinase (tk) gene. Based on the observation that tk deleted HSV-1 was limited to replicating in actively dividing cells, the researchers hypothesized that it may show selectivity for the gliomas while not causing pathogenesis in normal brain tissue (ameliorating neurotoxicity seen in earlier clinical trials). The data supported the potential of engineering and revolutionized the OV field (8).

Five years later, an engineered adenovirus was developed, with a deletion in the E1B locus. As the function of this protein is to bind and inactivate p53, this newly crippled virus requires a cell lacking functional p53 to replicate effectively. This virus, under the name Onyx-015, became the first engineered oncolytic virus to go to clinical trial (9).

While there is only one approved OV treatment in the United States, globally there are three approved therapies. In 2004, the first therapy was approved in Latvia, Georgia, and Armenia. Known as Rigvir, this virus is a wild-type ECHO-7 picornavirus. Although it was approved, there is not much information regarding its efficacy. The second virus is Oncorine/H101 which is a modified form of Onyx-015 that has been approved in China as of 2005. The virus approved in the United States as of 2015 is T-VEC or Imlygyic (10).

Like Martuza's virus, the base virus for T-VEC is HSV-1. However, unlike the tk deleted virus, T-VEC uses a different strategy for targeting tumor cells. T-VEC has a

double deletion and is lacking in both γ 34.5 and ICP47. The protein γ 34.5 blocks the PKR pathway. PKR is a cellular protein that detects cellular stressors and results in cellular shutdown and inhibition of viral replication. However, cancer cells often disrupt this pathway, such as Ras transformed cells encoding a PKR blocking protein. Therefore, a reliance on a dysfunctional PKR pathway is a potential selection method, which T-VEC uses.

However, time has also shown that being able to replicate is only part of the oncolytic virus story. The ability of the OV to recruit immune cells is also vital to its efficacy and the developers of T-VEC further increased the efficacy of their virus by deleting the ICP47 gene and replacing it with the immune stimulator granulocyte-macrophage colony stimulating factor (GM-CSF). As T-VEC replicates and lyses the tumor, it also produces a cytokine which recruits innate immune cells to the site of the tumor, ideally initiating a systemic immune response to newly released tumor antigens (1). This strategy has certainly proven successful for T-VEC in melanoma, both alone and in combination with other therapies.

Despite only three viruses being delivered to patients in the clinic, there are a wide variety of viruses employing various targeting mutations and immune stimulating transgenes. For HSV-1, the main mutation seems to be the double deletion of γ 34.5 and ICP47, although more work is being done on adding more mutations and widening the tumor range.

HSV-1 and Adenovirus, both of which have been successful, are double-stranded DNA viruses. Another double-stranded DNA virus family being explored are poxviruses, with vaccinia virus as the most popular candidate.

1.3 Vaccinia Virus Oncolytics

Among the double stranded DNA viruses, poxviruses are quite unique. These viruses replicate entirely in the cytoplasm, independent of cellular DNA replication mechanism and the nucleus. This means that the risk of integration is significantly lower than DNA virus that replicate in the nucleus and can go latent, like HSV-1(11). The genomes of these viruses are quite large, nearly 190 kb with 200 genes, and encode many proteins to assist with immune evasion and other supplementary functions in addition to the base requirements for an infectious virus. While this means that they do not replicate and lyse cells as fast as viruses like VSV, it does allow for more sophisticated engineering as there is more room for tumor targeting deletions and transgene insertions.

Vaccinia virus (VACV), one of the most well-known poxviruses second to smallpox, has been studied quite extensively during the development of a safer smallpox vaccine. In the 1980s and 1990s, prior to the engineering movement, wild-type vaccinia was able to induce remissions in cases of leukemia, myeloma and other carcinomas (12-14).

Just like the other viruses mentioned earlier, many engineered vaccinia viruses are being studied for oncolytic activity. Some of the modifications are similar to the others mentioned earlier, including but not limited to the deletion of TK and expression of immune stimulating molecules such as IFNβ and GM-CSF (15). Other mutations are unique to vaccinia such as the deletion of B18R, a gene product that neutralizes secreted interferons (16).

Despite multiple oncolytic vaccinia viruses being produced and being tested in clinical trials, none have made it to final approval. As a result, this study proposes a new vaccinia oncolytic and the benefits of its unique targeting strategy.

1.4 Novel Oncolytic Vaccinia Mutants

As mentioned above, vaccinia virus encodes many immune evasion proteins. One of these proteins is E3, encoded by the E3L gene. The carboxy-terminus of the E3 protein is able to bind dsRNA and inhibit sensing by PKR. Considering that T-VEC functions by making the virus sensitive to PKR, various mutants with partial or complete deletions of E3 were developed. Two of these mutants, VACV-E3LΔ83N and VACV-E3LΔ54N, which are highly attenuated in most cells and wild-type mice, were able to show selective replication in certain melanoma and breast cancer cell lines (17, 18).

In order to further characterize oncolytic potential, the viruses were tested in a human melanoma immunocompromised (SCID/bg) mouse model as well as an immunocompetent mouse breast cancer model. In the human melanoma model, complete clearance of the treated tumor as well as slight reduction of an adjacent tumor was seen. In the breast cancer model, tumor volume reduction was seen in both treated and untreated tumors. However, the method of selectivity for the mutant's replication was not known at the time of these studies.

1.5 Necroptosis and Vaccinia

Around 2007, researchers began to characterize a non-apoptotic cell death pathway dependent on the interaction of two kinases: RIPK1 and RIPK3 (19-22). While the name necroptosis was originally given to any programmed form of necrosis, it was

later adapted to be defined based on the formation of a complex known as the necrosome (23). Later on, more initiators of the necrosome beyond RIPK1 were discovered.

The essentials of the necroptosis pathway involve an initiator molecule such as RIPK1 interacting with the activator molecule RIPK3. This complex then recruits other molecules and forms a necrosome. The formation of the necrosome results in the phosphorylation of an effector molecule MLKL (mixed-lineage kinase-like pseudokinase). When MLKL is phosphorylated, it trimerizes and is transported to the cell membranes. At the membrane, MLKL forms pores resulting in loss of membrane integrity and an explosive cell death phenomenon (24, 25).

Our lab identified another necroptosis initiating molecule, DAI. DAI is a cellular stress sensor and can bind to Z-form nucleic acids. DAI is also able to interact with RIPK3 through a common RHIM domain and initiate necroptosis. Part of E3's function in vaccinia virus infections is to inhibit this necroptosis pathway by binding the z-form nucleic acids and preventing DAI sensing. The vaccinia E3 mutants are less pathogenic due to DAI activating necroptosis and inhibiting viral replication (24). Therefore, it is possible that the necroptosis pathway is how the vaccinia mutants can be tumor selective.

1.6 Necroptosis and Cancer

Apart from its role as an antiviral cell death pathway, necroptosis and RIP3 expression is also highly relevant in oncology. Certain cytotoxic chemotherapeutic agents are thought to bypass resistance to apoptosis by utilizing the necroptosis pathway.

Ectopic expression of RIPK3 in tumor cells lines that have little to no endogenous RIPK3 expression sensitized the cells to death by etoposide, doxorubicin, paclitaxel, camptothecin, cisplatin and 5-fluorouracil (26).

Despite the data supporting RIPK3's role in augmenting chemotherapeutic efficacy, loss of RIPK3 expression is a widely-seen phenomenon in tumors. One study showed an absence of RIPK3 protein expression in approximately 66% of cancer cell lines, with low expression in 20% of hematopoietic cancers and 80% of the others tumor types (26). Although the majority of this thesis work is focused on breast cancer and melanomas, RIPK3 low tumor targets exist in many cancer subtypes, increasing the potential scope of this research.

One hypothesis for why there is a loss of RIPK3 is that the promoter is epigenetically silenced due to hypermethylation. Research has shown that treatment with hypomethylating agents 5'-aza-2'-deoxycytidine or 5'-azacytidine recapitulates RIPK3 expression and rescues sensitivity to TNFα and zVAD mediated necroptosis (26). One proposed mechanism for how this hypermethylation occurs in tumors is the presence of 2-hydroxyglutatarate (2-HG). The function of citric acid cycle enzyme isocitrate dehydrogenase is to convert isocitrate into α-ketoglutarate. However, when cells contain mutated IDH, such as IDH1 R132H, isocitrate is converted to 2-HG. This molecule inhibits TET2 activity, leading to hypermethylated DNA. Treatment with 2-HG can lead to reduction in RIPK3 expression and decrease sensitivity to TNFAand zVAD mediated necroptosis. These IDH mutants are seen in various tumors types: gliomas, AML, cholangiocarcinoma, certain sarcomas prostate, lung, and colon cancer (27). However, it is important to note that methylation and IDH dependent loss of RIPK3 is only one facet

of this story as there may be other pathways leading to a loss of RIPK3 in tumor cell lines.

While an initial correlation between RIPK3 expression and oncolytic efficacy has been seen in vivo with two different human patient melanoma samples (data not published), it does not account for the cell line specific differences that may contribute to variations in tumor growth and response to the oncolytic. A matched-pair of tumor cell lines, RIP3 positive/negative would be a more appropriate model. Therefore, a secondary goal of this study is to develop these matched pair cell lines for future work.

1.7 CRISPR-Cas9

Originally isolated from Staphylococcus bacteria, CRISPR-Cas9 was optimized to edit mammalian cells. The underlying principle relies on two main parts: Cas9 and a guide RNA (gRNA). A gRNA is complementary to a certain gene segment and The Cas9 enzyme utilizes a guide RNA that targets a specific region of the genome and induces double-stranded breaks. These breaks most commonly repair themselves through non-homologous end joining (NHEJ) which introduces errors and renders the gene nonfunctional. Therefore, by delivering Cas9 and a gRNA specific to a gene of interest, the gene can be knocked out.

There are two methods of delivering these components. Transient transfections allow short-term expression. However, for the production of stable cell lines, the components must be integrated into the genome utilizing lentiviral transduction. These vectors are single-replicating, indetende to integrate the gene of interest and stop replicating. Lentivirus vectors are based on HIV integrating proteins yet use a rhabdovirus envelope, such as VSV-G, in order to enhance tropism of the virus. The

components of the lentiviral genome are stored on separate plasmids, depending upon the generation.

Second generation lentiviruses have three plasmids. The lentiviral transfer plasmid has the LTR and gene of interest. This can be easily manipulated to deliver transgenes or small RNAs such as guide RNAs. The envelope plasmid contains the envelope protein (such as VSV-G) and the packaging plasmid has the HIV proteins TAT, REV, GAG and POL. Third generation lentiviruses split this even further. The transfer plasmid has a modified LTR that doesn't need TAT. The packaging plasmid is split into two, one for REV and one for GAG and POL. Separating the lentivirus on more plasmids increases the safety of the virus yet reduces the yield since the cell needs to be transfected with more plasmids (28)

While labs often develop their own lentivirus and guide RNA through molecular cloning, this system has also been highly commercialized by companies specializing in plasmid construction such as Addgene and GenScript. One such system sold by these companies is the LentiCRISPR system, developed by Dr. Feng Zhang's lab to deliver a guide RNA and Cas9 in a single lentivirus. This system was then optimized to the LentiCRISPRV2. As an additional safety option, they developed the Lentiguide-Puro, which is analogous to LentiCRISPRV2, but is lacking Cas9 and is used in cells already containing the enzyme. This plasmid also confers puromycin resistance for selection of transduced cells (29).

1.8 Cancer Models

As seen in the literature, the loss of RIPK3 occurs in multiple cancer types. Therefore, while this study primarily focuses on melanoma, breast cancer and some

preliminary work with glioblastoma, the penultimate goal is to expand the work to other RIPK3 deficient cancer types.

The cancer lines studied here can be separated into two categories. The first are human-derived tumors which would be studied in vivo utilizing immunocompromised mice. SKBr3 is an ER negative, PR negative, HER2 positive breast adenocarcinoma derived from pleural effusion. T-47D is an ER positive, PR intermediate, HER2 negative breast adenocarcinoma derived from pleural effusion. HS578T is an ER negative, PR negative, HER2 negative ductal carcinoma derived from pleural effusion (30). While MDA-MB-435S was originally thought to be a breast cancer cell line (18). it is actually a melanoma line. PANC-1 is a pancreatic cancer cell line isolated from a pancreatic carcinoma of ductal cell origin. U118 is a grade IV glioblastoma/astrocytoma. U251 is a grade III-IV astrocytoma. U87 and U343 are glioblastomas of unknown grade and origin.

However, as referenced earlier, the immune response is necessary for true oncolytic efficacy. Therefore, five murine lines will be studied for the development of immunocompetent tumor models. For the BALB/C mouse background, JC and 4T1 are two breast cancer lines. 4T1 models a stage IV triple-negative breast cancer, which has the worst clinical prognosis in humans. K7M2 is an osteosarcoma lung metastasis model. Cells used in this study were K7M2 transduced with luciferase. For the C57BL/6 background, the E0771 triple negative metastatic breast cancer and B16 melanoma were chosen for study.

1.9 Aim of Study

The overall aim of the study is to characterize the role of necroptosis in oncolytic efficacy of VACV E3 mutants. This will be done with two subsections. First, the status of necroptosis in a variety of cancer cell lines will be characterized and patterns between necroptosis and oncolytic efficacy analyzed. Second, the actual functionality of the necroptosis pathway, mainly RIP3 expression, will be manipulated by molecular editing techniques, to provide a more specific look at the role of RIP3 in changing oncolytic efficacy.

CHAPTER 2

MATERIALS AND METHODS

2.1 In Vitro Cancer Cell Culture

Human HT-29 colorectal carcinoma cells were obtained from ATCC (ATCC HTB-38) and cultured in McCoy's 5a medium supplemented with 10% FBS. Human HS578T breast cancer cells were obtained from ATCC (ATCC HTB-125) and cultured in DMEM supplemented with 10% FBS and 0.01 mg/ml bovine insulin. Human HS578Bst breast epithelial cells were obtained from ATCC (ATCC HTB-125) and cultured in DMEM supplemented with 10% FBS and 30ng/ml human EGF. Human T-47D breast cancer cells were obtained from ATCC (ATCC HTB-133) and cultured in RPMI 1640 supplemented with 10% FBS. Human SKBr3 breast cancer cells were obtained from ATCC (ATCC HTB-30) and cultured in McCoy's 5a medium supplemented with 10% FBS. Human pancreatic cancer PANC-1 cells were obtained from ATCC (ATCC CRL-1469) and cultured in DMEM supplemented with 10% FBS. Human glioblastoma cell lines U251, U118 and U87 were maintained in MEM supplemented with 5% FBS. Human glioblastoma U343 cells were maintained in DMEM supplemented with 5% FBS.

Murine B16 melanoma cells and K7M2-luc osteosarcoma cells were cultured in DMEM medium supplemented with 10% FBS. K7M2-luc were a gift from the Blattman lab and are transduced with luciferase for *in vivo* imaging. Murine E0771 and E0771-Cas9 breast cancer cells were cultured in RPMI 1640 supplemented with 10% heat-inactivated FBS. Murine 4T1 breast cancer cells were cultured in RPMI supplemented

with 10% FBS. Murine JC breast cancer cells were cultured in RPMI supplemented with 10% FBS.

All aforementioned cell lines were grown in atmospheric air with 5% CO_2 at 37_0C. Human MDA-MB-435S melanoma cells were obtained from ATCC (ATCC HTB-133) and were cultured in Leibovitz's L-15 medium supplemented with 10% FBS, 2 mM L-glutamine and 0.01 mg/ml bovine insulin. These cells were grown at 37_0C with no CO_2.

2.2 Necroptosis Dye Exclusion Assay

Cells of interest were cultured in 12 well microscopy plates in base media overnight to allow adherence to plate. Base media was then swapped out for media supplemented with the blue DNA dye Hoescht at a concentration of 2 ul/ml, the red cell death dye propidium iodide at a concentration of 2ul/ml and pan-caspase inhibitor zVAD. For human lines, SMAC mimetic LCL161 was also added to this media. After one-hour treatment, wells were supplemented with another dose of zVAD and cell death inducer TNFα. Cells were allowed to incubate, four hours for murine cell lines and six to eight hours for human cell lines.

Parental VACV is the western reserve (WR) strain. VACV-E3L mutants were produced from the wild-type WR virus by deleting the entire E3L locus and inserting the N-terminus deleted E3L copy with in vivo recombination and X-gal selection.

For VACV induced necroptosis, murine cells were pretreated with mouse IFNα for 16 to 18 hours. Cells were infected with a MOI of 5 of VACV-E3LΔ83N or VACV-E3LΔ54N and rocked for one hour. After one hour, cells were overlaid with media containing Hoescht and propidium iodide. Cells were allowed to incubate for six hours as VACV induced necroptosis is a slower process.

Images were taken at 10X and quantified with an EVOS microscope. The Hoescht signal was captured with a DAPI filter cube and the Propidium iodide signal was captured with an RFP filter cube. Images displayed are an overlay of the Trans UV, DAPI and RFP images. Cell death quantification was measured as % viability (total cells-dead cells/ total cells) with technical replicates. Graphs were created in Excel and standard deviation utilized for error bars.

2.3 SDS-Page and Western blot

Cells of interest were cultured in base media in 6 and 12 well microscopy plates. For DAI and RIP3 blots, cells were treated with universal or murine IFNα for 16 to 18 hours. For pMLKL and MLKL aggregation, cells were infected with various VACV mutants or treated with zVAD and TNFα at the concentrations used for microscopy and harvested six hours post infection.

Lysates were prepared by scraping cells then centrifuging for 1,000 g for 10 minutes. Pellets were resuspended in RIPA lysis buffer (25mM Tris•HCl pH 7.6, 150mM NaCl, 1% NP-40, 1% sodium deoxycholate, 0.1% SDS) and incubated on ice for 10 minutes. Proteins were reduced by adding Laemmli buffer and DTT and run through a 10% polyacrylamide gel (7.5% polyacrylamide gel for MLKL aggregation) at 70 volts and 120 volts upon reaching the separating gel. Proteins were then transferred to PVDF membranes in transfer buffer (25 mM Tris, 192 mM Glycine) for 60 minutes at 60 volts at 4C (20 hours at 20V at 4C with 1X CAPS buffer, 20% methanol for MLKL aggregation). PVDF membranes were allowed to dry overnight and then rehydrated with methanol.

Blots were blocked in freshly prepared 5% non-fat milk or BSA in TBST. After a quick wash, blots were blocked in primary antibody diluted in 3% non-fat milk or BSA in TBST overnight at 4C. Blots were washed and incubated with secondary antibody in non-fat milk for one hour. Human DAI antibody (NBP1-7684), human RIPK3 (CST E1Z1D), mouse RIPK3 (CST D4G2A), mouse total MLKL (CST D6W1K), and mouse phosphorylated MLKL (CST D6E3G) was probed with anti-Rabbit IgG HRP conjugated secondary. Mouse DAI antibody (Zippy) was probed with anti-mouse IgG HRP conjugated secondary. Blots were coated in a chemiluminescent substrate for two minutes and visualized with x-ray film. After initial probing, the PVDF membranes were stripped with stripping buffer (62.5 mM Tris-HCl pH 6.8, 2% SDS) supplemented with 30 µl β-mercaptoethanol per 10 ml stripping buffer at 50 C. Blots were then blocked and incubated with a different primary or probed for actin loading control (sc-47778, an HRP-conjugated primary antibody).

2.4 VACV Plaque Assay

Murine cells were plated in 12 well plates to reach 90% confluency at time of infection. They were treated with or without mouse IFNα for 16 to 18 hours prior to infection. Cells were then infected with a MOI of 5 of VACV, VACV-E3LΔ83N, or VACV-E3LΔ54N in 100 ul of MEM 2% FBS per well. After one hour of rocking, the cells were washed three times with media. One set of wells were harvested at this time point and the other set was harvested 24 hours later. Virus was harvested by scraping cells into the media, conducting three freeze thaws at -80$_0$C and sonication. Virus samples were quantified by plaque assay in a monolayer of BSC-40. Duplicates of each sample were plated onto monolayers with 6 different dilutions and stained 48 hours later with

crystal violet. Plaques were counted and the resulting titers determined. Plaque assays were done with either single replicate (no error bars) or in biological triplicate (error bars). Graphs were created in Excel or Graphpad Prism and standard deviation utilized for error bars.

2.5 Hypomethylation Assays

Cells of interest were cultured in base media in 12 well microscopy plates for five hours to allow cell settling. 5'-Azacytadine (5-AZA) was formulated at 10mM in DMSO and stored at -20C. At the time of treatment, 5-AZA was diluted in base media and added dropwise to cells. Every 24 hours, media was replaced, and 5-AZA dilutions were freshly prepared and added to cells. Cells were grown in 5-AZA media for 36 hours before treatment for necroptosis microscopy and harvest for SDS-Page/Western blot. Cell death quantification was done with technical replicates. Graphs were created in Excel and standard deviation utilized for error bars.

2.6 Bacterial Plasmid Preparation

The pLentiguide-Puro lentivirus transfer plasmid with RIPK3 gRNA was obtained from GenScript. 800 pg in 2ul was used to transform NEB Stbl3 and JM109 e. coli using heat shock. Cells were initially grown in SOC media for an hour before colony isolation on Ampicillin supplemented LB plates. Colonies were used to create bacterial glycerol stocks. DNA was isolated for confirmation using the Qiagen Mini-prep kit. Upon confirmation of successful plasmid transformation with nanodrop quantification and XhoI restriction digest, the Qiagen 500 kit (Maxi-Prep) was used to prepare plasmid DNA stock for transfection.

2.7 Production of Lentivirus

293TLx cells were brought up from liquid nitrogen stocks and passaged twice. Cells were then plated in 6 well plates at a confluency of 70% at the time of transfection. Plasmids were mixed at equimolar ratios in serum-free DMEM, Fugene HD was added to the mixture at a 6:1 ratio and incubated for 20 minutes. pCMV-VSV-G was a gift from Bob Weinberg (Addgene plasmid # 8454; http://n2t.net/addgene:8454; RRID: Addgene_8454). psPAX2, given to our lab by Ana Lemos of Dr. Grant McFadden's lab, was originally a gift from Didier Trono (Addgene plasmid # 12260; http://n2t.net/addgene:12260; RRID: Addgene_12260).

The media of the 293TLx cells was changed and the plasmid mixture was added dropwise. At 16- and 24-hours post-transfection, the media was partially changed twice to base media supplemented with the antibiotic-antimycotic (anti-anti) solution from Thermo Fisher. At 40- and 64-hours post-transfection, media containing lentivirus was collected and stored at 4C. Lentivirus media was then filtered with a 0.22-micron filter, concentrated using the Lenti-X kit and aliquoted in 293T media supplemented with anti-anti.

2.8 Lentivirus Transduction

E0771 cells were plated in a 24 well plate with base media to reach 40% by transduction time where media was aspirated. Lentivirus particles were diluted in base media to a final volume of 250 ul and added to each well. The Dharmacon Cas9 lenti was diluted to a MOI of 0.3. The guide RNA lentivirus particles were serially diluted from undiluted to 10^{-9} in E0771 media. After 4 to 6 hours after transduction, 750 ul of media was added to the well and the cells were incubated in the BSL-2 room for 48 hours. After that, the cells were selected with blasticidin or puromycin at E0771 lethal doses to allow

for selection of transduced cells. Cell stocks were prepared, and the cells were evaluated for expression of specific products by various methods.

2.9 Immunofluorescence

Verification of Cas9 stable expression was done through immunocytochemistry. E0771-Cas9 were plated in BioLite 12 well clear bottom plates. After removal of media, cells were fixed with 2% formalin in PBS for 10 minutes. After washing three times with PBS, cells were permeabilized with 0.2% Triton X-100 in PBS. After another three PBS washes, cells were blocked with 2% BSA in PBS for 10 min. The mouse primary antibody against Cas9 (NBP2-36440) was added at a dilution of 1:500 in 2% BSA in PBS. The plate was incubated overnight at 4C, washed with PBS and incubated with an anti-mouse secondary conjugated to Alexa 488 (Invitrogen A11001) for one hour. The slips were washed for another 10 minutes and incubated with DAPI DNA stain for 15 minutes. The wells were visualized under the EVOS microscope with the DAPI and GFP filter cubes.

CHAPTER 3

RESULTS

3.1 Characterization of Necroptosis by Western Blot Analysis

The initial step of characterizing the cell lines for necroptosis was to look for pathway protein expression by SDS-Page and Western blotting under reduced conditions. The first two proteins assayed were DAI and RIP3. As DAI has interferon-inducible expression in certain cell lines, all cell lines were tested with or without pre-treatment with Type I interferon α (IFN α). Universal IFNα was used for human cell lines. HT29, a human colon cancer line, was used as a positive control for necroptosis as the line has been previously characterized in the literature and experimentally.

Although DAI has multiple isoforms, the expected band size of both DAI and RIP3 is between 42-60 kDa. For all of the human cancer cell lines, a band in the expected size range for DAI was seen in all samples, melanoma, breast cancer, and glioblastoma. None of the human lines had an increase in DAI expression after interferon treatment. However, there was variability among cell lines in RIP3 expression. In breast cancer, SKBr3 was the only RIP3 positive cell line whereas T-47D and HS578T were both RIP3 negative. The melanoma cell line MDA-MB-435S was RIP3 negative whereas the pancreatic cell line PANC-1 and all the glioblastoma lines U343, U251, U118 and U87 were all RIP3 positive. As a control comparison, the matched pair non-tumor line HS578Bst was RIP3 positive. None of the human cell lines had interferon dependent variablity in RIP3 expression.

As murine studies have been important for generating pre-clinical support for oncolytic virotherapy and immunocompromised mice with human tumors are not

sufficient to understand the complete mechanism, multiple mouse origin tumor lines were simultaneously assayed. Mouse IFNα was used and L929, a mouse fibroblast cell line, was used as the necroptosis positive control. As K7M2 was characterized after reproducible results from E0771 and B16, they were used as control cell lines in certain experiments rather than L929 cells.

DAI expression increased in response to interferon treatment in the breast cancer lines E0771 and 4T1 and the melanoma B16. However, both the breast cancer line JC and osteosarcoma K7M2 had a constitutive expression of DAI that was not increased by stimulation with interferon. There was also variability in RIP3 expression. The breast cancer lines E0771 and JC were RIP3 positive. Conversely, the breast cancer line 4T1, melanoma B16, and osteosarcoma K7M2 were RIP3 negative.

3.2 Characterization of Necroptosis with TNFα/zVAD and VACV E3L Mutant Induced Cell Death

While DAI and RIP3 expression can indicate that the proteins are being expressed in the cells, the functionality of the pathway as a whole must be assayed by looking at whether the cells could undergo death by the necroptosis pathway. Tumor-necrosis factor α (TNFα) is a cytokine that can induce cell death pathways such as apoptosis and necroptosis. However, to isolate necroptosis, a caspase-independent pathway, the pan-caspase inhibitor zVAD-fmk (zVAD) was added to the treatment. For the human cell lines, previous work on HT29 has shown that a SMAC inhibitor such as LCL161 is also needed to enhance necroptosis (26). The cells were treated for 6-8 hours prior to imaging.

As necroptosis is a porous death that causes loss of membrane integrity, living cells can be differentiated by uptake or exclusion of dyes such as propidium iodide, read in the RFP range and visualized as red. A baseline count of cells for comparison was measured by Hoechst, a DNA stain read in the DAPI range and visualized as blue. Hoescht does not require permeabilization for uptake, so it was used to mark live and dead cells. Combing these reagents provided a way that total cell count (blue) could be compared visually against how many dead cells (red) underwent necroptosis.

HT29, the RIP3 positive cell line control line, had an increase in red/propidium iodide staining between mock and the TNFα/zVAD/LCL161 treated cells. The RIP3 positive breast cancer SKBr3 also had an increase in red/propidium iodide staining, albeit not as much as other cell lines. The three RIP3 negative cell lines MDA-MB-435S, HS578T, and T-47D showed no difference in morphology or red/propidium iodide staining between the mock and treated cells. The RIP3 positive glioblastoma cell lines U118, had an increase in red/propidium iodide staining between mock and treated cells. However, the RIP3 positive pancreatic cancer PANC-1 line and the other three RIP3 positive glioblastoma lines had no change in morphology or red/propidium iodide staining between the mock and treated cells.

While the TNFα/zVAD/LCL161 combination was included to isolate necroptosis alone, an extra verification that the cell death being visualized is necroptosis further validates the findings. Representative RIP3 positive cell line HT29 and RIP3 negative cell line T-47D were used for validation. Cells were again untreated or treated with TNFα /zVAD/LCL161 to induce necroptosis, but the third group of cells was pretreated with GSK872, a RIP3 kinase inhibitor before induction of necroptosis.

Looking at the dye exclusion assay images for HT29, there is an increase in red/propidium iodide staining between the untreated and TNFα /zVAD/LCL161 cells. However, there is a decrease in red/propidium iodide staining analogous to mock when the cells were pretreated with GSK872. For the RIP3 negative breast cancer T-47D, there is no change in morphology or red/propidium iodide staining between the mock and either of the treated cell groups.

Just like the human cell lines, the necroptosis pathway in murine lines was assayed by dye exclusion assay. However, for the murine lines, mouse TNFα was utilized, no LCL161 was needed and cell death occurred faster allowing for imaging at 4 hours post-TNFα.

L929, the RIP3 positive cell line control line, had an increase in red/propidium iodide staining between mock and the TNFα/zVAD treated cells. RIP3 positive breast cancers E0771 and JC also had an increase in red/propidium iodide staining. Conversely, RIP3 negative breast cancer 4T1, melanoma B16, and osteosarcoma K7M2 did not have a change in red/propidium iodide staining or morphology between the mock and treated cells.

Unlike TNFα, which utilizes the RIP1-RIP3 pathway, VACV is believed to utilize the DAI-RIP3 pathway to induce necroptosis. Therefore, to look at necroptosis induced by VACV E3L mutants, cells were pretreated with IFNα prior to infection to increase the expression of DAI.

E0771, the RIP3 positive breast cancer, had an increase in red/propidium iodide staining between mock and the TNFα/zVAD treated cells, as well as in cells that were infected with VACV-E3LΔ54N and VACV-E3LΔ83N compared to mock. Both RIP3

negative melanoma B16 and osteosarcoma K7M2 had no change in red/propidium iodide staining in any of the conditions. Debris was seen in all cell lines treated with VACV-E3LΔ54N, making it likely as a result of background residue present in the virus sample and not as an indication of necroptosis.

3.3 VACV Induced MLKL Phosphorylation and Trimerization by Western Blot Analysis

Further confirmation of necroptosis occurring is the phosphorylation and trimerization of the necroptosis effector protein Mixed Lineage Kinase Domain Like Pseudokinase (MLKL). This process occurs right before membrane pores and loss of integrity and therefore the presence of phosphorylated and trimerized MLKL detected by western blot can be utilized to determine whether necroptosis has been induced. Representative cell lines, RIP3 positive E0771, and RIP3 negative K7M2 were assayed for changes in MLKL, with L929 fibroblasts with and without TNFα/zVAD treatment as the necroptosis controls.

MLKL is a protein of approximately 50 kDa. Phosphorylated MLKL was assayed under reduced conditions with a 10% SDS-Page gel, and western blot optimized with BSA for phosphorylation detecting antibody. Trimerized MLKL was assayed under non-reducing conditions with a lower 7.5% SDS-Page Gel, transferred at a lower voltage for longer, and detected at greater than 150 kDa band with a non-phosphorylated MLKL antibody.

Phosphorylated MLKL was detected in the L929 TNFα/zVAD lane, but not the untreated L929 lane (Fig. 8a lane 2 and lane 1) supporting the specificity of the antibody. For the RIP3 positive E0771 cells, only cells treated with TNFα/zVAD (Fig.8a lane 9) and cells pretreated with IFNα and infected with VACV-E3LΔ83N (Fig. 8a lane 8) had a

band for phosphorylated MLKL. For the RIP3 negative K7M2 cells, none of the lanes had a band for phosphorylated MLKL (Fig. 8b).

Trimerized MLKL at 150 kDa was detected in the L929 TNFα/zVAD lane, but not the untreated L929 lane. While MLKL monomers of 50 kDa were detected in untreated L929, there was a decrease in monomer expression in the TNFα/zVAD treated cells (Fig. 9 lane 1 and 2). For the RIP3 negative K7M2 cells, none of the lanes had a 150 kDa band for trimerized MLKL. However, they all had the expression of the 50 kDa MLKL monomer (Fig. 9 lanes 3-9).

3.4 Vaccinia Single-Step Replication Growth Curves

As one of the requirements of an effective oncolytic virus is the ability to replicate in target cells, the comparative ability of VACV and the VACV-E3L mutants was assayed using single-step growth curves. After infection with a high MOI of 5 in various cell lines, virus samples were collected, and crystal violet plaque assays were to quantify growth as a change in pfu/ml over a 24-hour growth period.

The human cell lines were assayed by previous members of the lab. RIP3 status was annotated according to Fig. 1 and literature (31). Experiments in immunocompromised mice showed that VACV-E3LΔ83N was too pathogenic. Only VACV-E3LΔ54N was used in these assays instead of both of the mutants. VACV was able to replicate to a Δtier of at least 10_7 pfu/ml in the human breast cancers HS578T, MCF-7, T-47D, and SKBr3 and in the normal matched line HS578Bst. It was also able to replicate to at least 10_5 pfu/ml in the human breast cancer MDA-MB-468. Conversely, VACV-E3LΔ54N had variable replication. The mutant was able to replicate in RIP3 negative HS578T, MDA-MB-435S, and T-47D. It was not able to replicate in RIP3

positive normal line HS57Bst or RIP3 positive breast cancer SKBr3. The mutant was able to replicate in breast cancer MCF-7 and not in breast cancer MDA-MB-468, but the RIP3 status of those lines has not confirmed experimentally by western blotting at this point (Fig. 10).

The ability of VACV and VACV-E3L mutants were not previously characterized in the murine cell lines E0771, B16 and K7M2. Therefore, single-step growth curves were also conducted in these lines. However, as DAI is the predicted sensor for VACV nucleic acids and DAI expression required interferon in these three cell lines, samples were assayed with or without mouse IFNα pretreatment. Both mutants were looked at as candidates in murine lines. The first set of assays were conducted without biological replicates and compared VACV to VACV-E3LΔ83N only.

VACV was able to replicate to a Δ titer of at least 10_7 pfu/ml in all the cell lines, regardless of interferon treatment. For RIP3 negative lines, the difference in VACV-E3LΔ83N growth in response to interferon was not much. For B16 melanoma, the Δ titer dropped from 5.54 * 10_7 pfu/ml to 6.59 * 10_6 pfu/ml after interferon treatment. For the K7M2 osteosarcoma line, the Δ titer dropped from 6.80 * 10_6 pfu/ml to 3.30 * 10_6 pfu/ml (Fig. 11a and 11b).

In order to further analyze the mutants' replication, the ability of E0771 to restrict replication of both VACV-E3LΔ54N and VACV-E3LΔ83N was assayed utilizing biological replicates. VACV was able to replicate at equivalent levels regardless of interferon. As seen in the previous assay, VACV-E3LΔ83N replication was reduced in E0771 interferon treated cells. For VACV-E3LΔ54N, the virus was able to replicate in untreated E0771 cells, but pretreatment with interferon inhibited replication entirely (Fig.

11c). There was a difference in replication inhibition between the two VACV-E3L mutants.

3.5 Summary of Results for Figures 1-11

In order to better visualize the correlation between RIP3/DAI expression, necroptosis pathway and VACV replication, the results from the first six figures were summarized into Table 1 for human cell lines and Table 2 for the murine cell lines. As mentioned earlier, data for the human cell line VACV replication as well as data for L929, JC, and 4T1 VACV replication was extrapolated from experiments done by previous lab members (18, 24, 32, 33).

For all human cell lines except for PANC-1, U343, U251, and U87, positive RIP3 expression resulted in positive necroptosis by dye exclusion. For those four cell lines, positive RIP3 expression did not result in positive necroptosis and propidium iodide uptake. For the cell lines for which VACV replication data was available, RIP3 positive cell lines SKBr3 and HS578Bst inhibited VACV-E3LΔ54N replication and RIP3 negative cell lines HS578T, T-47D and MDA-MB-435S did not inhibit VACV-E3LΔ54N replication.

For all of the murine cell lines, positive RIP3 cell lines matched with positive necroptosis by TNFα/zVAD and the opposite for negative RIP3 cell lines. For the three cell lines, E0771, B16 and K7M2, where necroptosis by VACV-E3L mutants was assayed, the data matched the TNFα/zVAD results. None of the RIP3 negative cell lines were able to inhibit VACV-E3L mutant replication, regardless of DAI expression or interferon treatment. The DAI constitutive breast cancer JC was able to reduce VACV-E3L mutant replication without interferon treatment. However, the DAI interferon-

inducible breast cancer E0771 and control fibroblast line L929 required interferon pretreatment to inhibit the replication of the VACV-E3L mutants.

In order to better understand the specific role of RIP3 and test whether RIP3 would be a good biomarker for VACV-E3L mutant oncolytic efficacy, two experimental strategies to create RIP3 positive/negative matched pair cells were explored. The two strategies were to increase RIP3 expression in RIP3 negative cells or cause a loss of RIP3 expression in a RIP3 positive cell.

3.6 Effect of Hypomethylation on RIP3 and Necroptosis

To investigate the hypothesis that hypermethylation causes loss of RIP3 expression in cancer cells, cells were treated with hypomethylating agent 5-Azacytidine (5-AZA) for multiple days. The first assay was sensitivity to TNFα/zVAD necroptosis. 5-AZA caused a decrease in red/propidium iodide and an increase in cell viability in the RIP3 positive control cell line L929 fibroblasts. 5-AZA caused no change in red/propidium iodide or cell viability in the K7M2 line (Fig. 12a and 12b). Changes in RIP3 expression was then assayed through western blot analysis. RIP3 was expressed in all L929 lanes, in untreated and all 5-AZA treated lanes (Fig. 12c, lanes 1-4). RIP3 was not expressed in the untreated or any of the 5-AZA treated K7M2 lanes (Fig. 12c, lanes 5-12).

3.7 CRISPR-Cas9 RIP3 Knockout in E0771 Cells

Utilizing C57BL/6 syngenic metastatic breast cancer line E0771, the creation of matched pair, stable RIP3 positive/negative cell lines was done utilizing the CRISPR-Cas9 gene-editing tool with lentiviral vectors.

Stable Cas9 expression, blasticidin resistant lentivirus particles were ordered from Dharmacon. The plasmid map for the lentivirus genome is indicated in Figure 13a. E0771 cells were transduced and cells were passaged in media containing blasticidin for selection and frozen down without sorting for Cas9 expression.

Confirmation of Cas9 expression was done with immunocytochemistry utilizing a Cas9 primary antibody and a rabbit secondary conjugated to a GFP fluorophore. DAPI was utilized as an indicator of DNA and to visualize nuclei. Green staining indicates Cas9 expression and blue staining indicates nuclei. Some cells have clear green staining around the nuclei (Fig. 13b). Some less distinct, web-like green staining is also present but controls lacking the primary antibody (not pictured here) also have web-like staining, implying that it is background noise from the secondary antibody.

In addition to stable Cas9 expression, guide RNA expression for the gene target is also necessary for a knockout. Lentivirus particles were made from the GenScript pLentiguide-Puro transfer plasmid, a derivative of the lentiCRISPRV2 system. The guide RNA used corresponded to the 4th exon of murine RIP3 (Fig. 14a)

E0771 cells were then transduced with the lentivirus particles and selected with puromycin containing media. The lentivirus was functionally titered by transducing cells with a serial dilution of lentivirus supernatant and looking at cell survival after puromycin selection. All of the untransduced cells died after puromycin addition. Cells transduced with undiluted supernatant had a complete monolayer of surviving cells. E0771 cells transduced with 10^{-1} supernatant had a confluence of approximately 40% surviving cells. E0771 cells transduced with 10^{-2} supernatant had a confluence of approximately 5% surviving cells. At a dilution of 10^{-3}, the well did not have any visible

surviving cells, similar to the untransduced well (Fig. 14b). The amount of puromycin resistant cells has a proportional relationship with the amount of viral supernatant used to transduce the cells.

Cells lacking RIP3 expression should lose sensitivity to TNFα/zVAD necroptosis. Therefore, dye exclusion assay of E0771-Cas9 cells with no gRNA virus, E0771 cells with Cas9 and gRNA after 24 hours of puromycin selection and E0771 cells with Cas9 and gRNA after 10 days of puromycin selection was used as an initial method to look at changes in necroptosis.

E0771-Cas9 cells with no gRNA lentivirus showed 17% viability after TNF/zVAD treatment. After transduction with gRNA and 24 hours of selection with puromycin, the E0771 cells had 23% viability after TNF/zVAD treatment. However, after 10 days of selection with puromycin, the cells had 45% viability after TNF/zVAD treatment. Transduction and selection decreased the sensitivity of the E0771 cells to TNF/zVAD (Fig. 16).

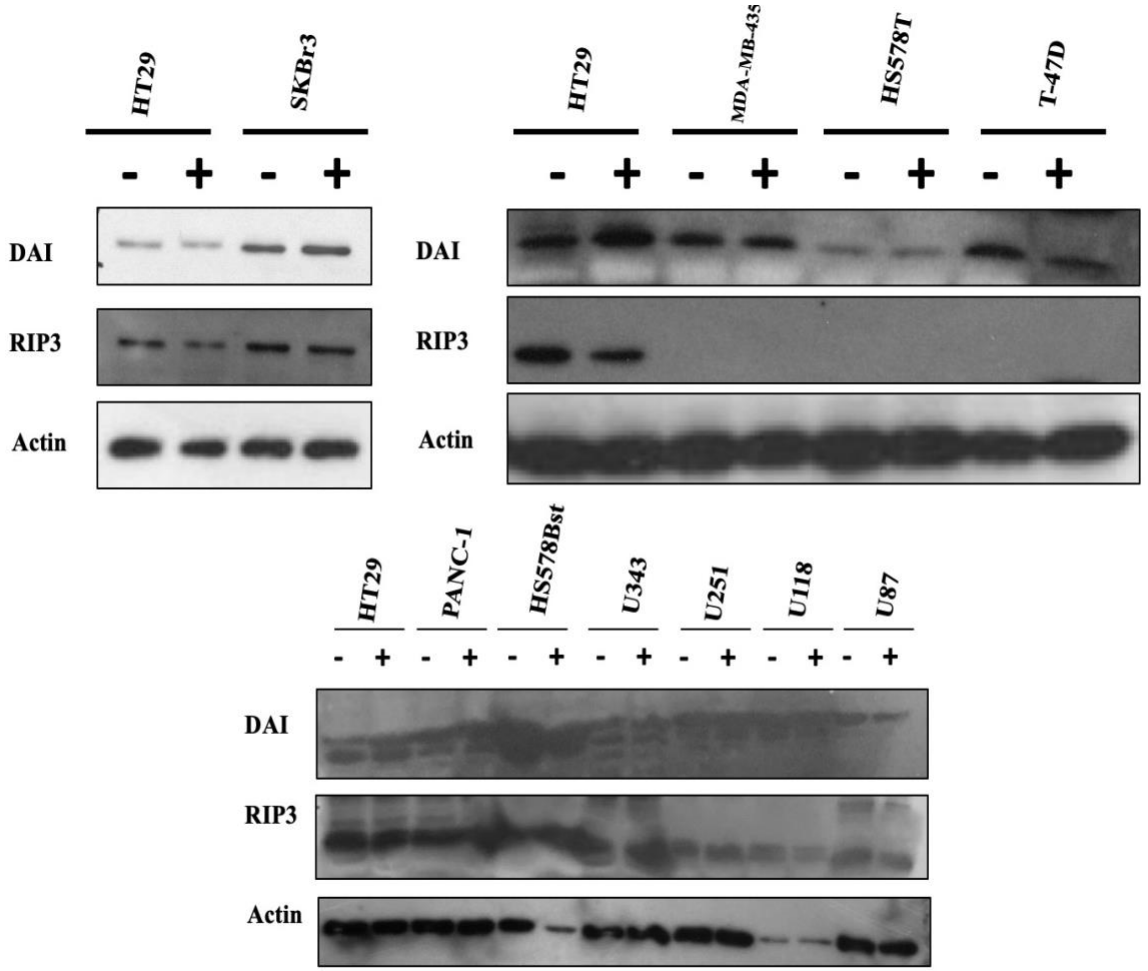

Figure 1: RIP3 and DAI expression in human cancer lines. Cells treated +/- universal IFNα 16-18 hours prior to harvest.

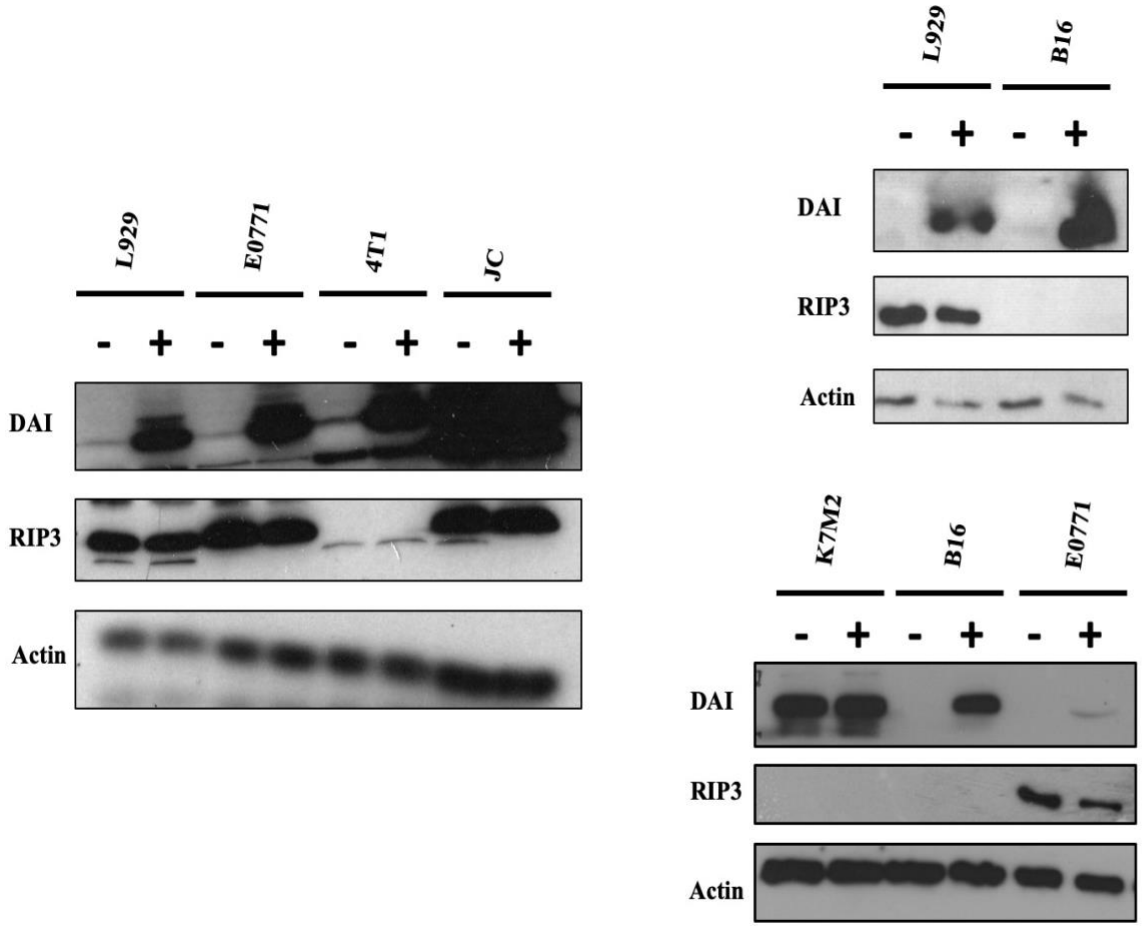

Figure 2: RIP3 and DAI expression in murine cancer lines. Cells treated +/- mouse IFNα 16-18 hours prior to harvest.

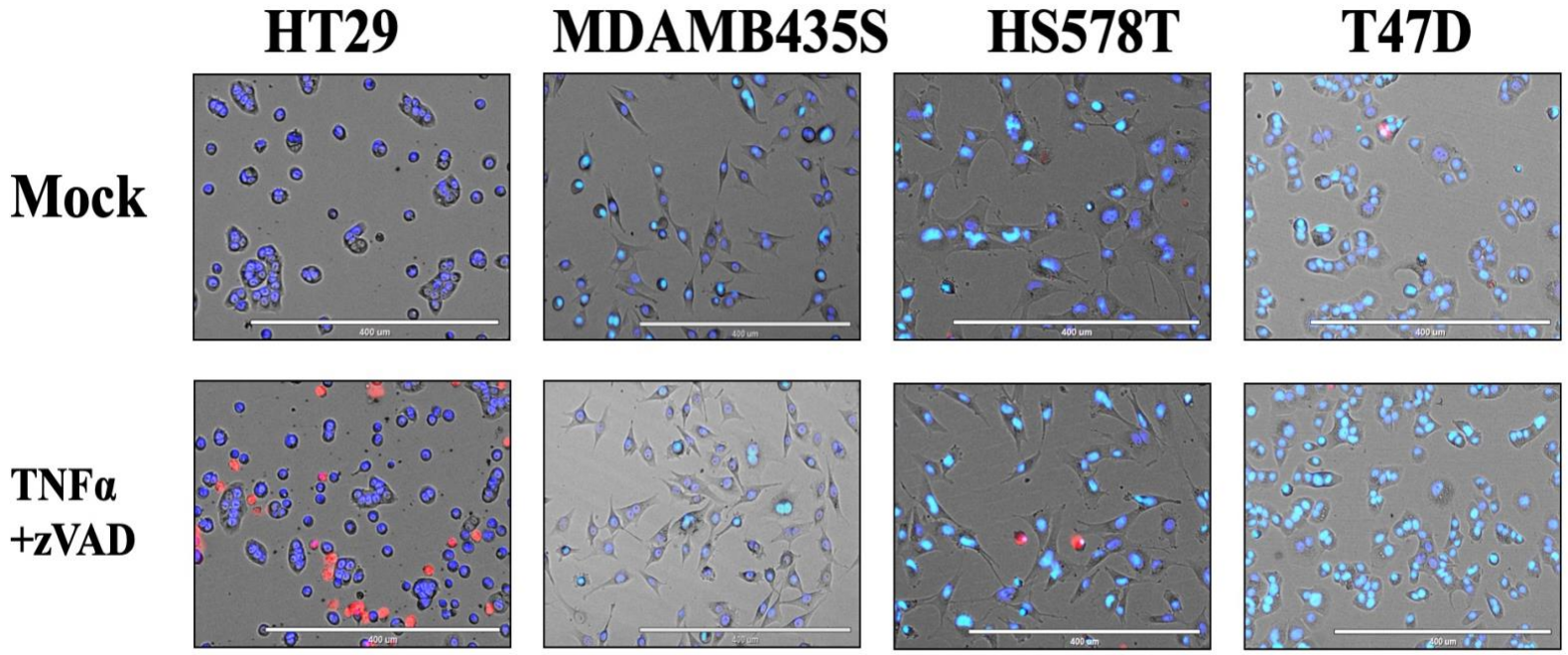

Figure 3: Fluorescent microscopy of human melanoma and breast cancer post treatment with TNFα, zVAD-fmk and SMAC mimetic, LCL161. Blue (Hoescht) represents nuclear staining and Red (Propidium Iodide) indicates cell death.

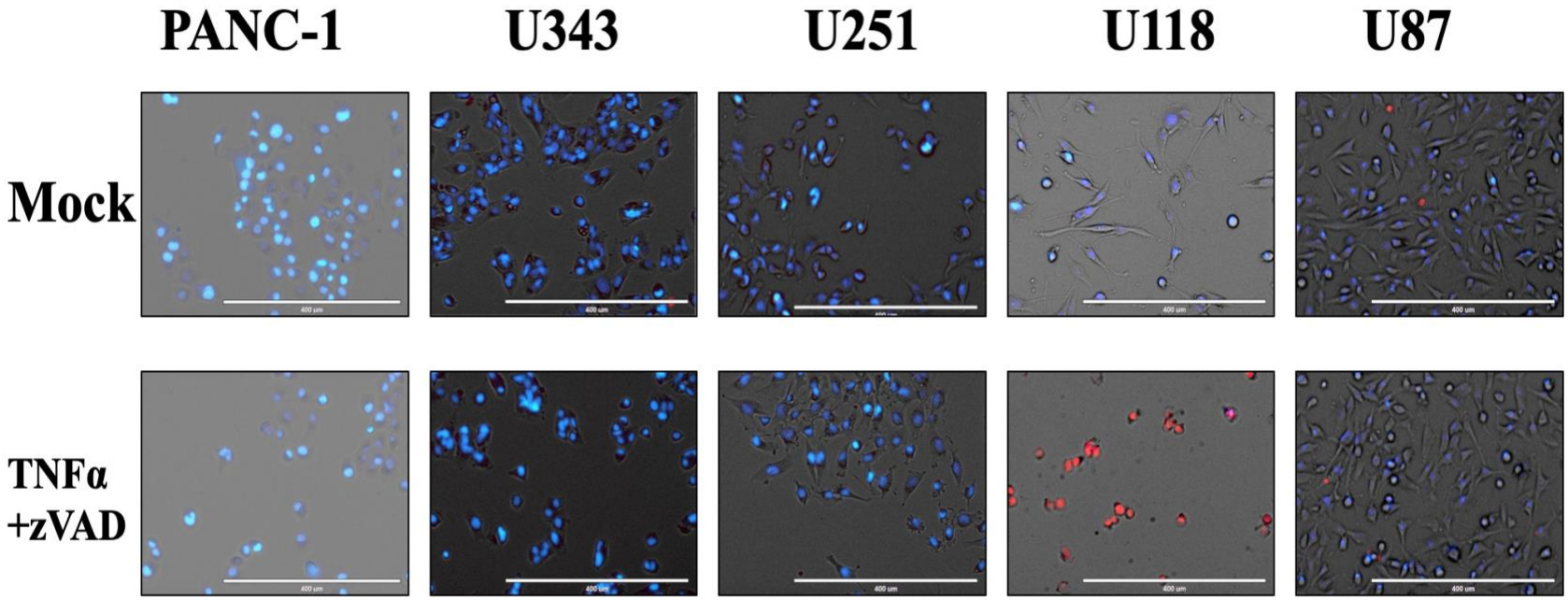

Figure 4: Fluorescent microscopy of human pancreatic cancer and glioblastoma post treatment with TNFα, zVAD-fmk and SMAC mimetic, LCL161. Blue (Hoescht) represents nuclear staining and Red (Propidium Iodide) indicates cell death.

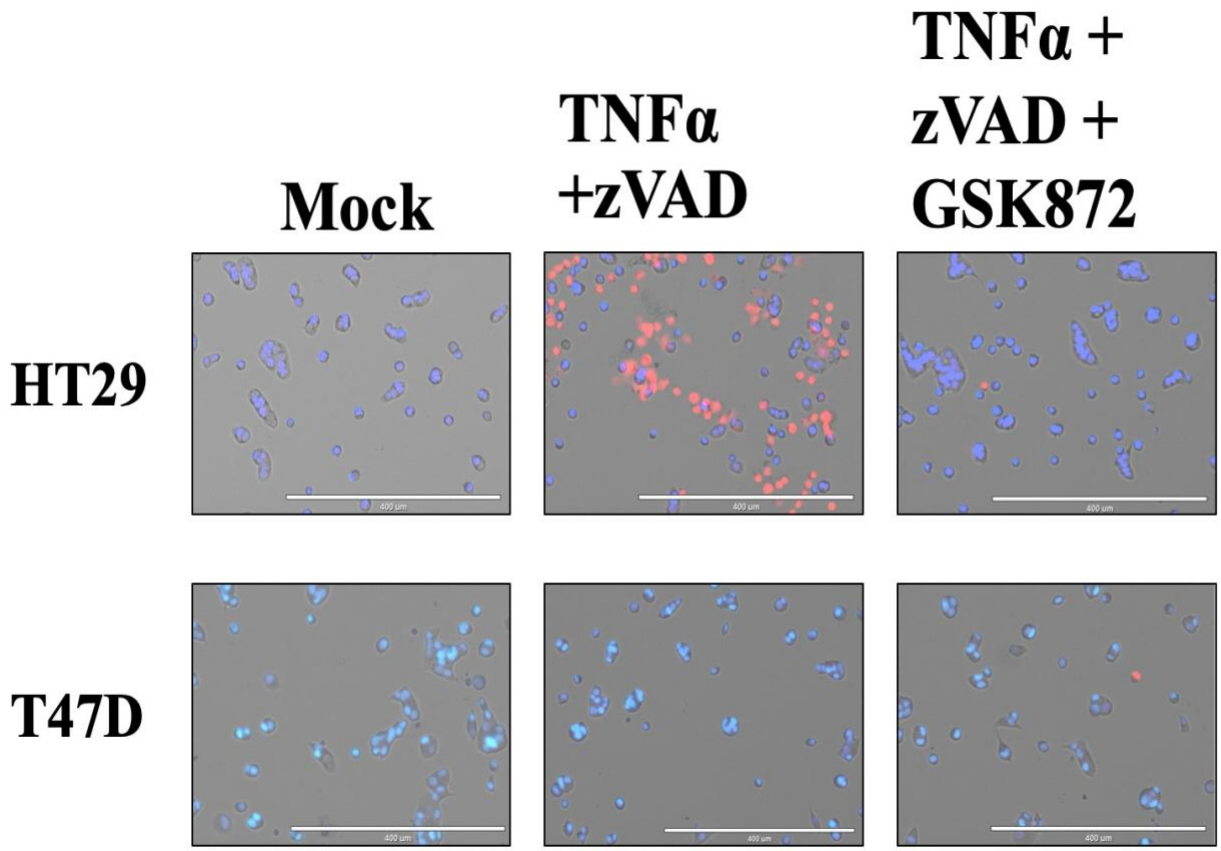

Figure 5: Fluorescent microscopy of representative human cancers post treatment with TNFα, zVAD-fmk and SMAC mimetic, LCL161, +/- RIP3 inhibitor GSK872. Blue (Hoescht) represents nuclear staining and Red (Propidium Iodide) indicates cell death.

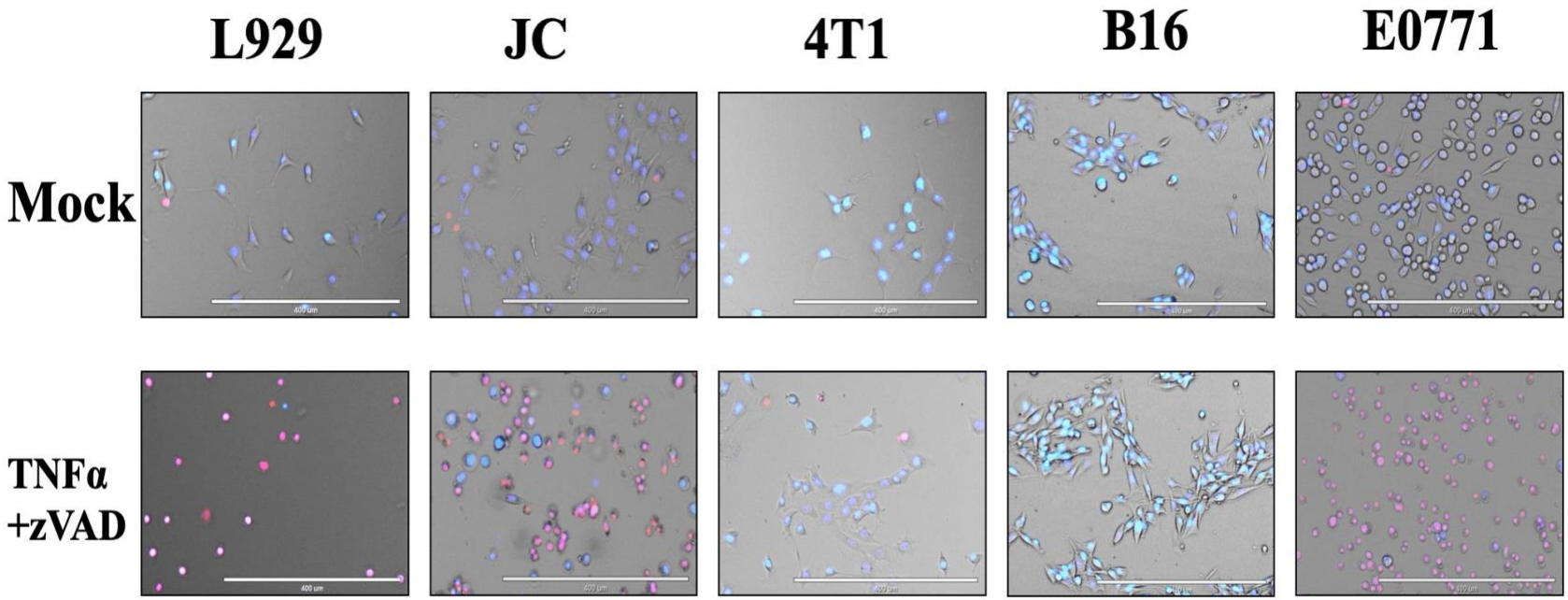

Figure 6: Fluorescent microscopy of mouse melanoma and breast cancer post treatment with TNFα and zVAD-fmk. Blue (Hoescht) represents nuclear staining and Red (Propidium Iodide) indicates cell death.

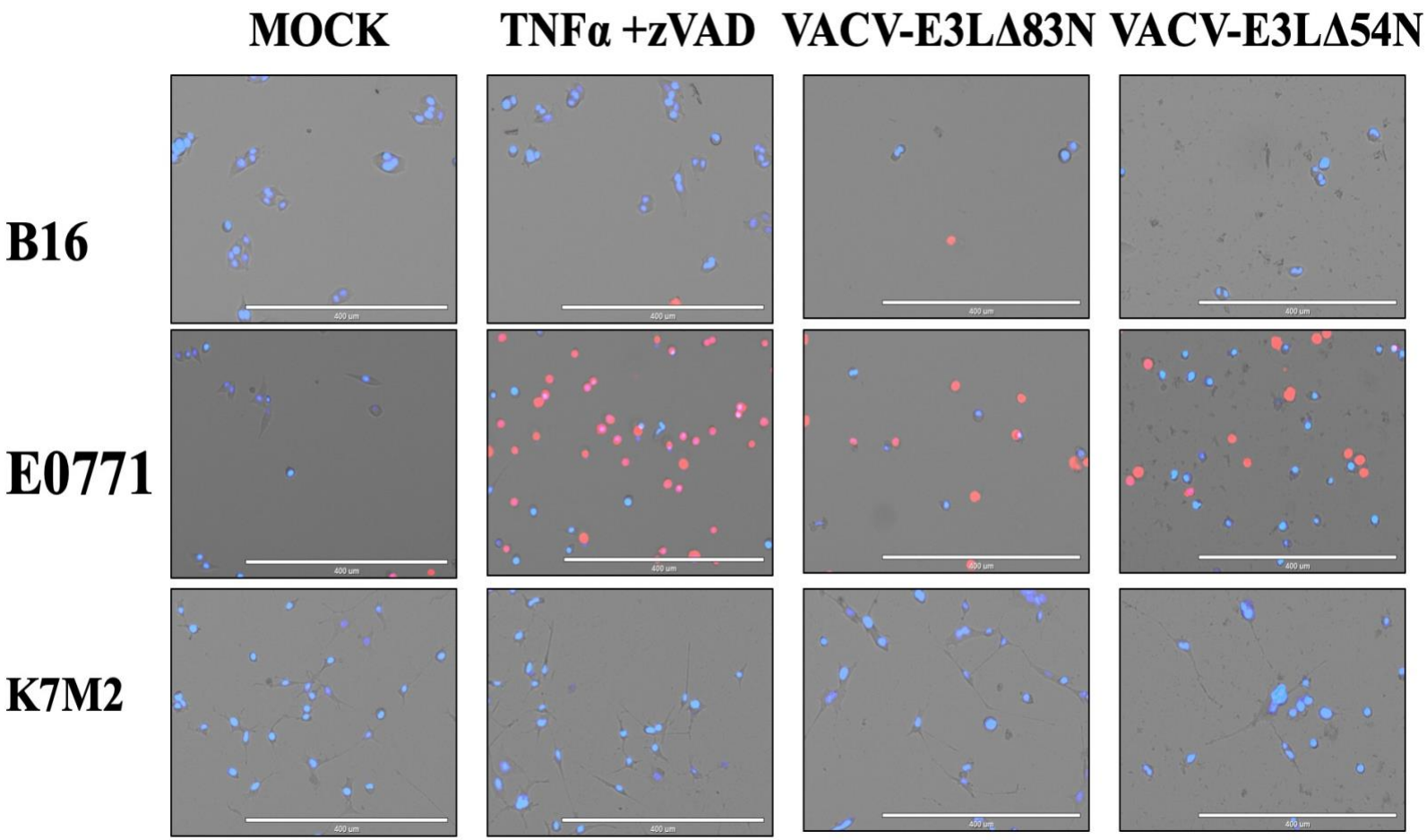

Figure 7: Fluorescent microscopy of mouse melanoma and breast cancer post treatment with TNFα and zVAD-fmk *or* VACV-E3L mutants and mouse IFNα. Blue (Hoescht) represents nuclear staining and Red (Propidium Iodide) indicates cell death.

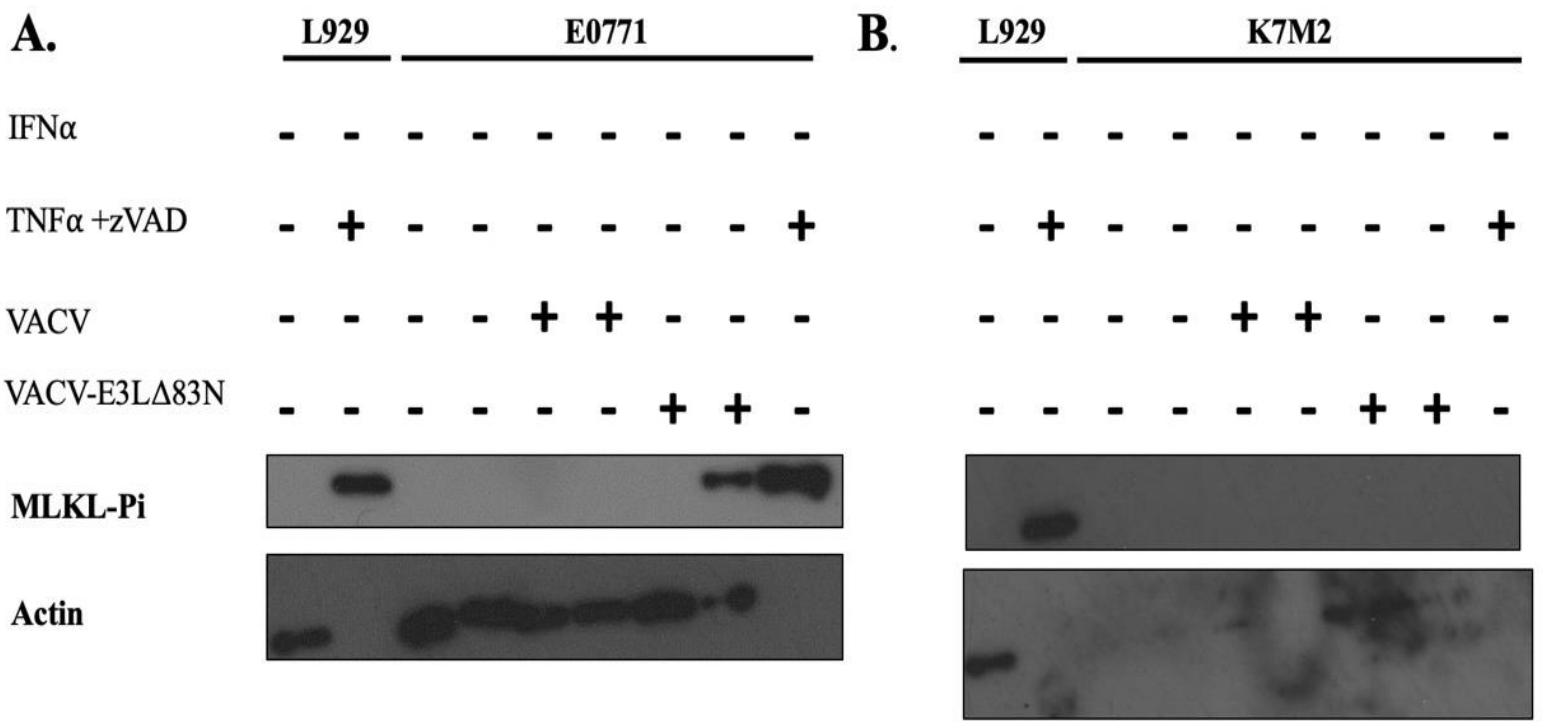

Figure 8: MLKL-Pi (Phosphorylated MLKL) expression in murine cancer lines. Cells treated/infected with mouse universal IFNα, TNFα/zVAD and VACV as indicated. **A)** RIP3 positive E0771 breast cancer **B)** RIP3 negative K7M2 osteosarcoma

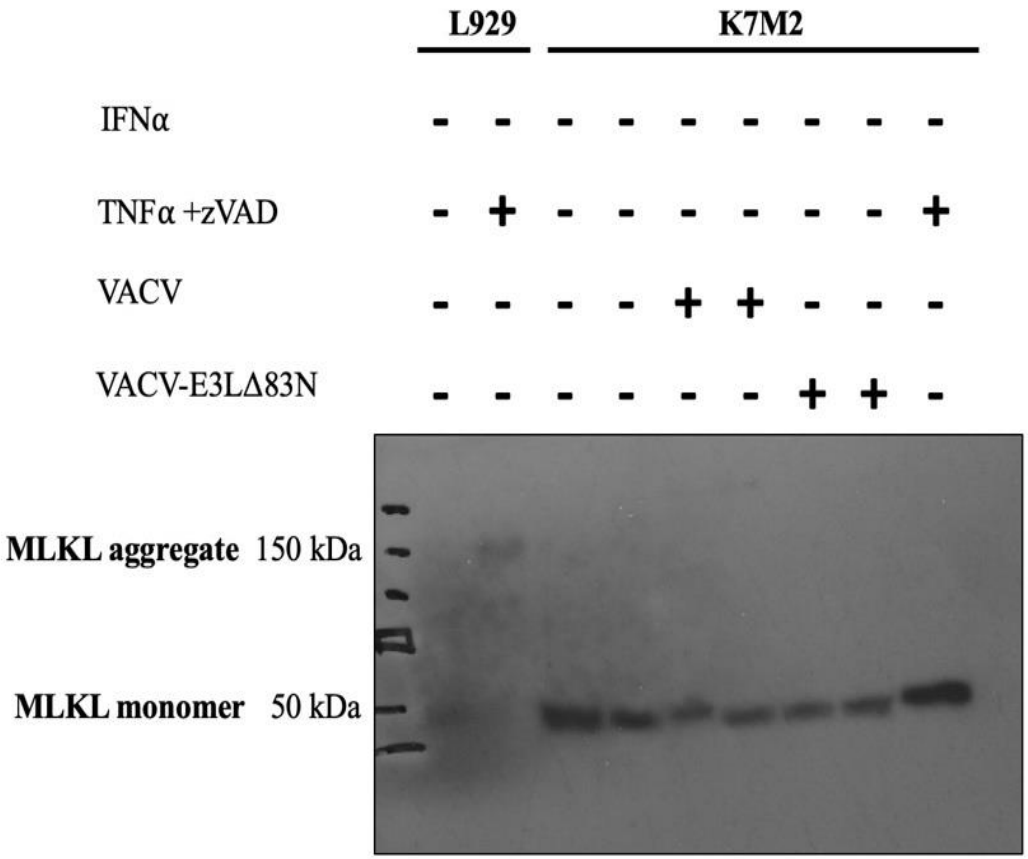

Figure 9: MLKL aggregate and monomer expression in murine K7M2 osteosarcoma. Cells treated/infected with mouse universal IFNα, TNFα/zVAD and VACV as indicated.

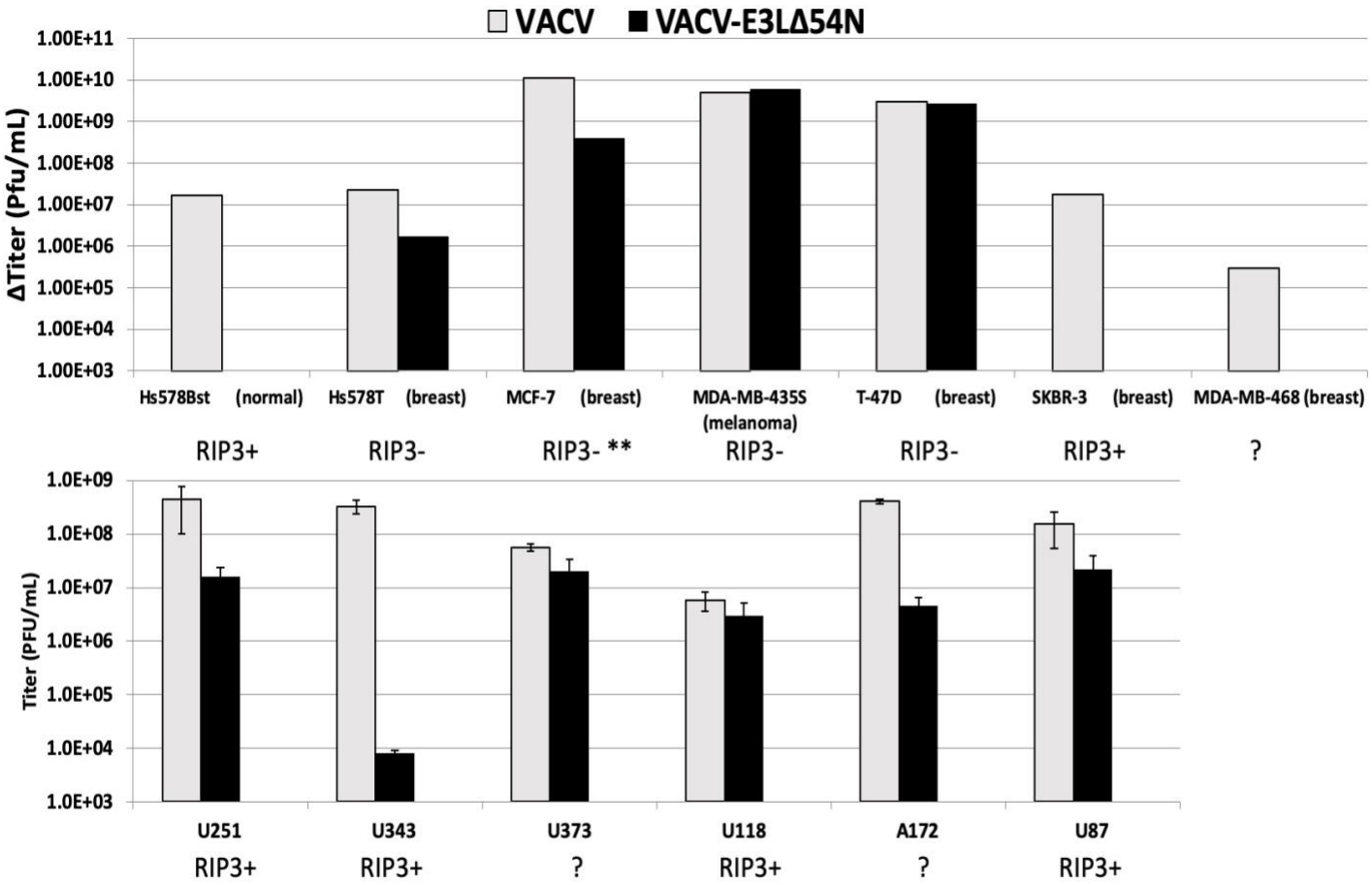

Figure 10: Adapted from Arndt et al. Single-step growth curves of VACV replication in human cancer cell lines. RIP3 Status from Fig. 1 displayed below respective cell lines. ** From literature

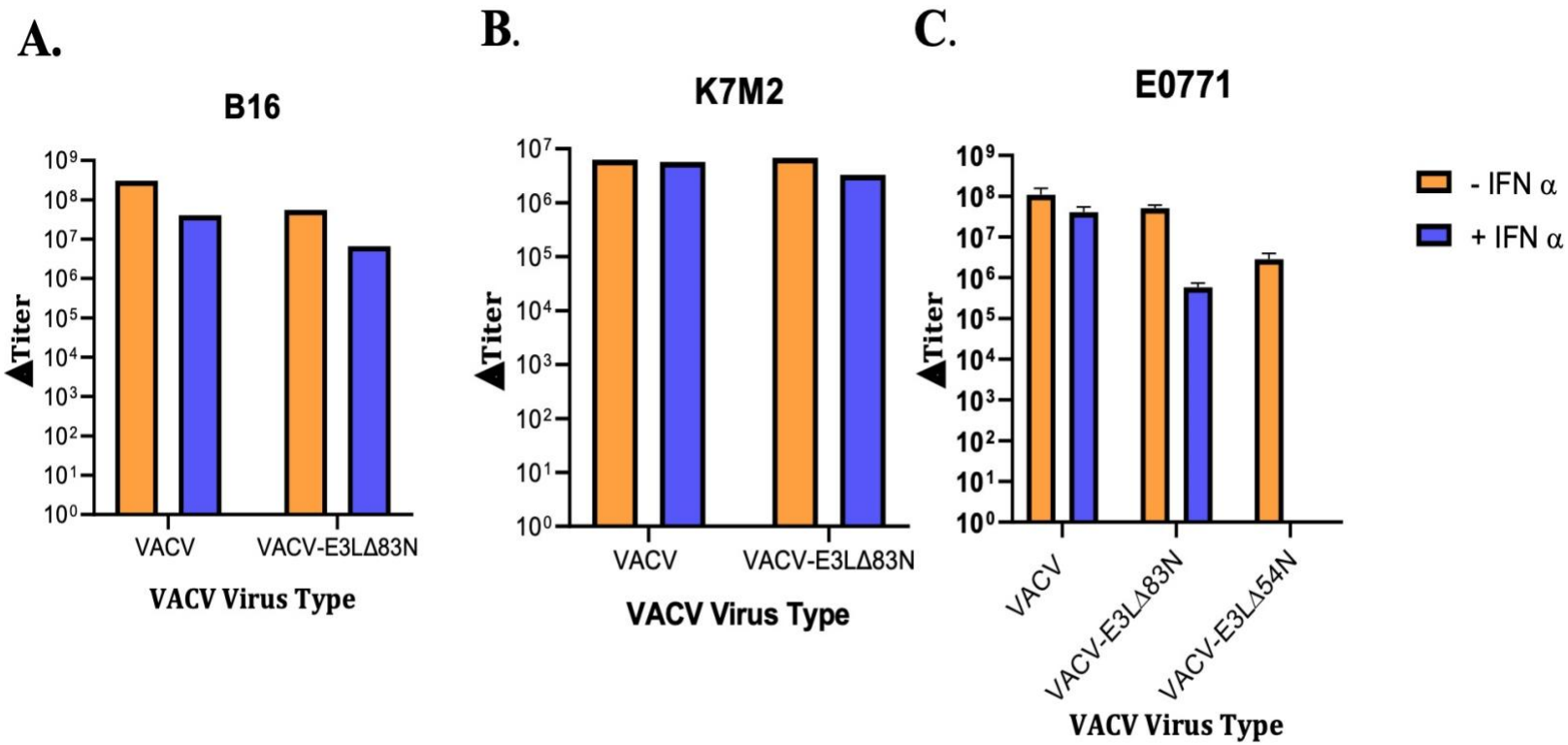

Figure 11: Single-step growth curves of VACV replication in murine cancer cell lines. Cells were pre-treated with IFNα 16-18 hours prior to infection with virus at MOI:5. Viruses were harvested at 0h and 24h. Resulting samples were tittered in BSC40 and 0-hour input was subtracted from 24 hour for change in titer. **A)** C57BL/6 melanoma B16 **B)** BALB/C osteosarcoma K7M2 **C)** C57BL/6 E0771 breast cancer

Table 1
Summary of Human Cell Line Results

Cell Line	Type	DAI	RIP3	Necroptosis by TNFα/zVAD	VACV Replication	VACV-E3L Mutant Replication
HT29	Colon Cancer	Constitutive	Positive	Positive		
SKBr3	Breast Cancer	Constitutive	Positive	Positive	Permissive	Inhibited
HS578Bst	Normal Breast Epithelia	Constitutive	Positive		Permissive	Inhibited
HS578T	Breast Cancer	Constitutive	Negative	Negative	Permissive	Permissive
MDA-MB-435S	Melanoma	Constitutive	Negative	Negative	Permissive	Permissive
T-47D	Breast Cancer	Constitutive	Negative	Negative	Permissive	Permissive
PANC-1	Pancreatic Cancer	Constitutive	Positive	Negative		
U343	Glioblastoma	Constitutive	Positive	Negative	Permissive	Reduced
U251	Glioblastoma	Constitutive	Positive	Negative	Permissive	Permissive
U118	Glioblastoma	Constitutive	Positive	Positive	Permissive	Permissive
U87	Glioblastoma	Constitutive	Positive	Negative	Permissive	Permissive

Table 2

Summary of Murine Cell Line Results

Cell Line	Type	DAI	RIP3	Necroptosis by TNFα/zVAD	Necroptosis by VACV-E3L mutants	VACV Replication	VACV-E3L Mutant Replication
L929	Fibroblast	Inducible	Positive	Positive		Permissive	Inhibited (with IFNα)
E0771	Breast Cancer (C57BL/6)	Inducible	Positive	Positive	Positive	Permissive	Reduced/Inhibited (with IFNα)
JC	Breast Cancer (BALB/C)	Constitutive	Positive	Positive		Permissive	Inhibited
4T1	Breast Cancer (BALB/C)	Inducible	Negative	Negative		Permissive	Permissive
B16	Melanoma (C57BL/6)	Inducible	Negative	Negative	Negative	Permissive	Permissive
K7M2	Osteosarcoma (BALB/C)	Constitutive	Negative	Negative	Negative	Permissive	Permissive

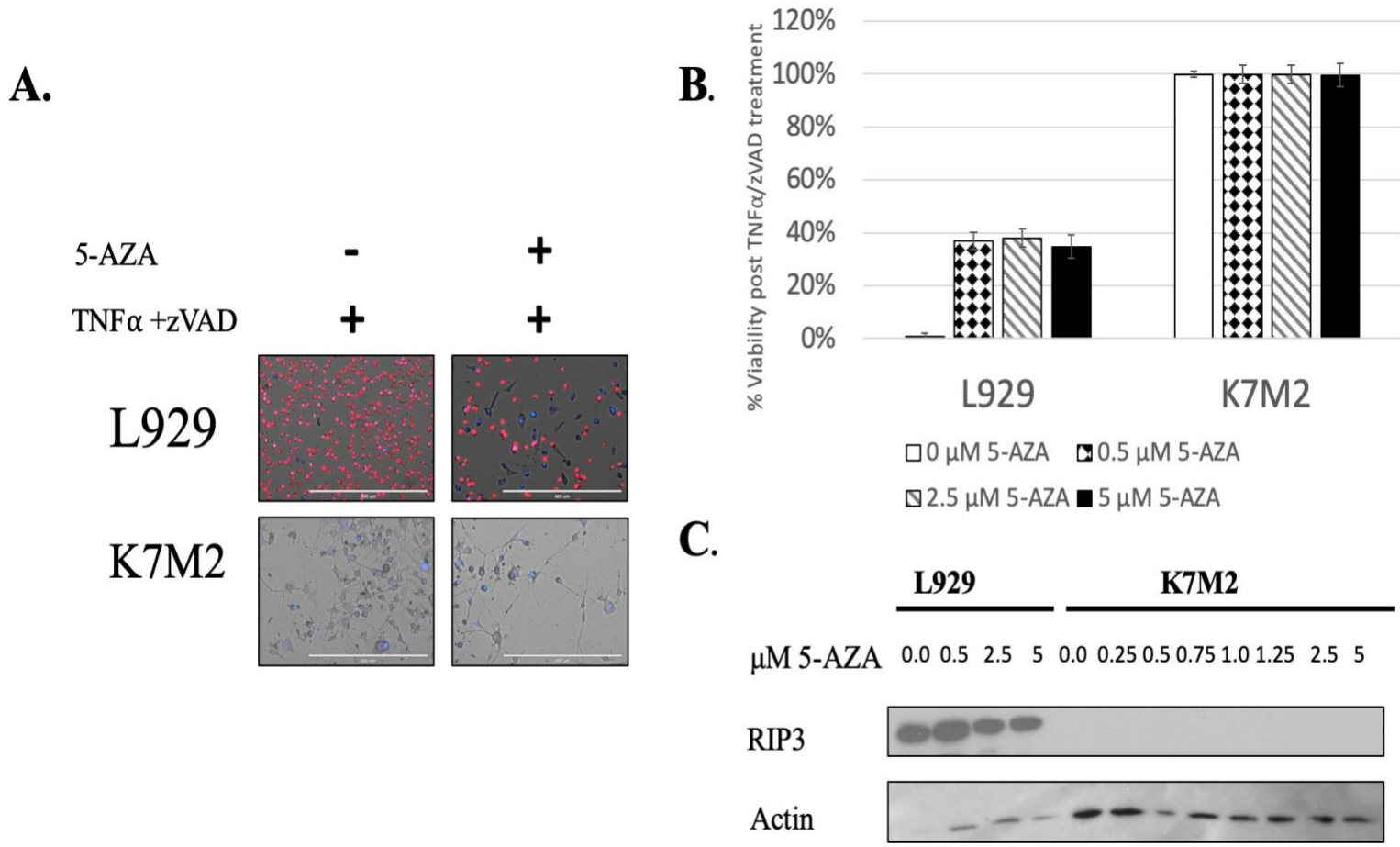

Figure 12: The effect of hypomethylating agent 5-AZA on murine cells lines. **A)** Cells treated with various doses of 5-AZA for 3.5 days prior to TNF/zVAD dye exclusion assay **B)** Quantification of dye exclusion assay for viability **C)** Western Blot analysis of RIP3 expression at each dose of 5-AZA

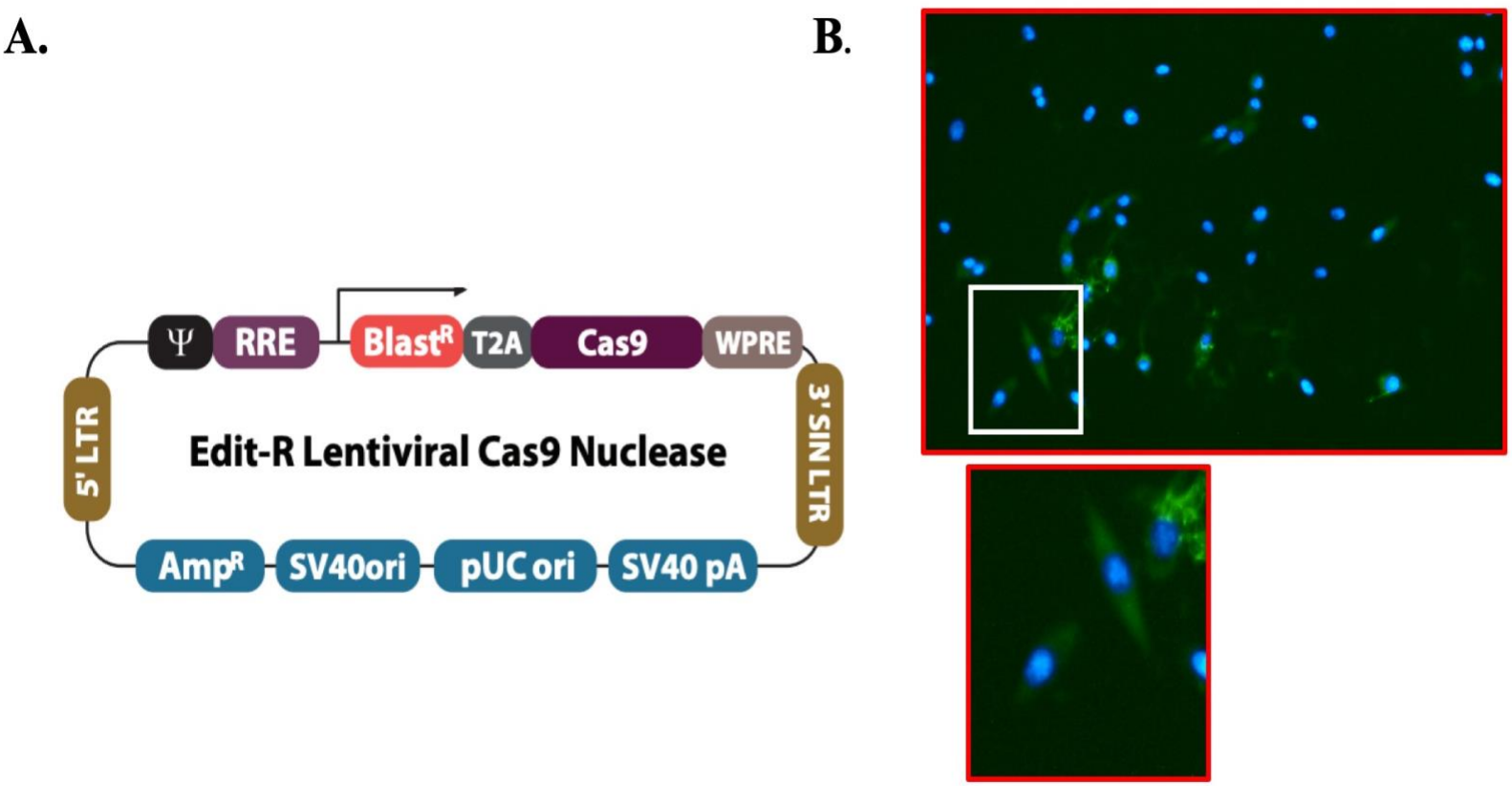

Figure 13: Expression of stable Cas9 in E0771 cells. **A)** Plasmid map for Dharmacon Cas9-Blasticidin lentivirus particles **B)** Detection of Cas9 expression in E0771-Cas9 cells by Immunocytochemistry. Green represents Cas9 expression and Blue represents nuclear staining by DAPI

A.

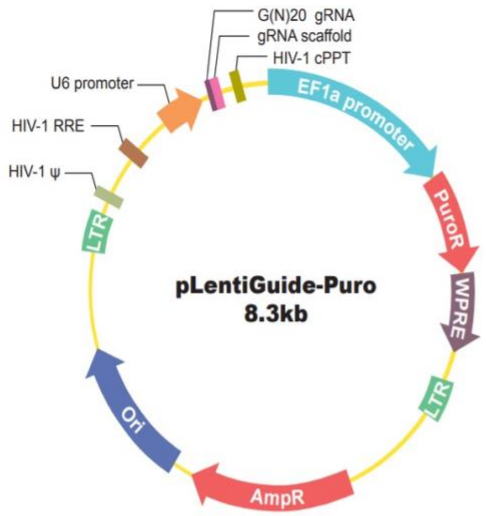

gRNA sequence:
TGGGGGCACCCTAGCGTACT

- Corresponds to exon 4 of mouse RIPK3

B.

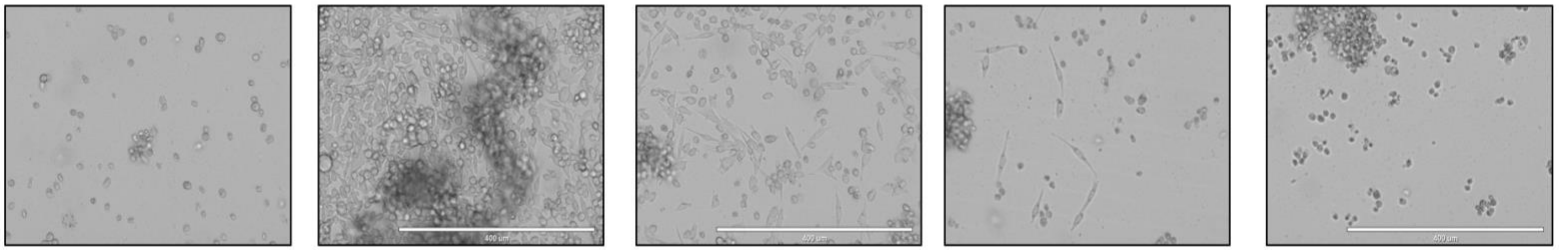

No Lentivirus **Undiluted** **10^{-1} virus** **10^{-2} virus** **10^{-3} virus**

Figure 14: Production of RIP3 guide RNA Lentivirus **A)** Plasmid map for Genscript pLentiGuide-Puro and gRNA sequence **B)** Lentivirus functional titer determined by serial dilution of viral supernatant and puromycin selection. Images taken on EVOS microscope

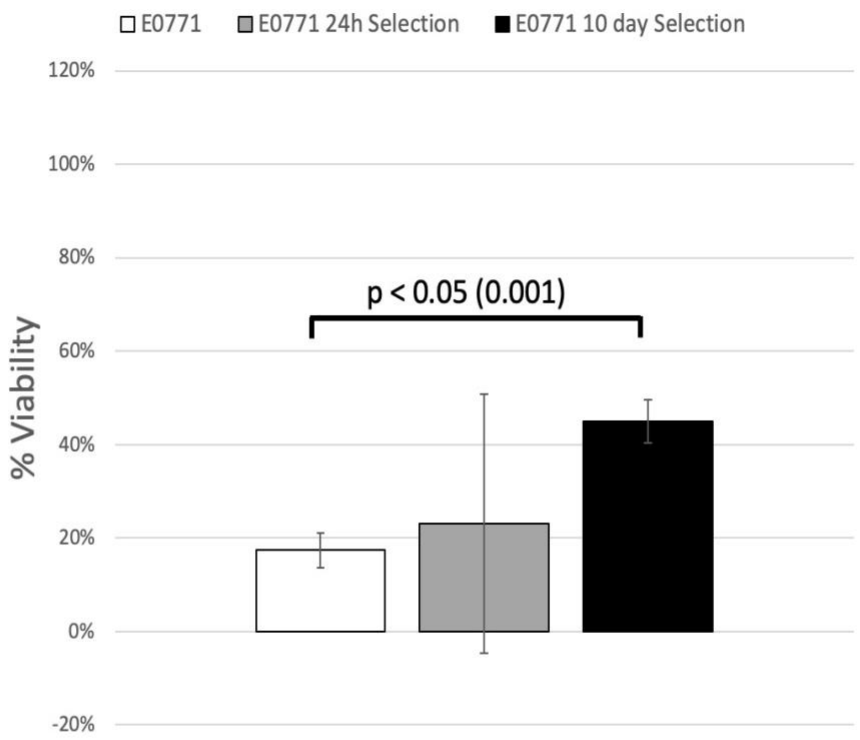

Figure 15: Quantification of TNF/zVAD dye exclusion assay for viability. The white column represents E0771-Cas9 cells with no guide RNA. The gray column represents E0771-Cas9-RIP3KO cells after 24 hours puromycin selection. The black column represents E0771-Cas9-RIP3KO cells after 10 days puromycin selection.

CHAPTER 4

DISCUSSION

The aim of this study was to characterize the role of the necroptosis pathway in the efficacy of two potential VACV based oncolytic viruses. Current frontrunners in the Oncolytic virotherapy field have indicated dependency on interferon dependent pathways deficiencies in cancer cells such as PKR. Since VACV's E3L gene is involved in inhibiting PKR signaling in host cells, primary in vitro work and mouse modeling indicated a potential for VACV with N-terminal deletions in the E3L locus as an oncolytic therapy. However, the data indicated that Ras and PKR alone did not fully explain the selectivity of VACV-E3LΔ54N and VACV-E3LΔ83N efficacy in various tumors (18). However, the ability of these viruses to replicate has also been attributed to the necroptosis pathway (24). In order to explore the hypothesis that the necroptosis pathway provides selectivity for oncolytic activity, various human breast cancers, melanomas, pancreatic cancers, and glioblastomas, as well as various mouse breast cancers, melanomas, and osteosarcomas, were assayed *in vitro*.

For necroptosis induction, two proteins with RHIM domains must interact. We first showed experimentally that the expression of the Z-form nucleic acid sensor DAI and necroptosis adaptor kinase RIP3 was not uniform across different cancer cell lines (Fig. 1 and 2).

While DAI was constitutively expressed in all human cancer lines assayed, the murine lines varied in whether interferon stimulation was required for DAI expression. RIP3 expression did not appear to be interferon dependent in any of the cell lines assayed, however, cancer cell type did not completely predict whether RIP3 was

expressed. Breast cancers were the most variable, with two of the three human lines being RIP3 negative but only one of the three murine breast cancers being RIP3 negative. Both the human and mouse melanomas in this study were RIP3 negative, but other primary melanoma samples not included in this data set have been characterized as RIP3 positive. The lung metastatic murine osteosarcoma line K7M2 was RIP3 negative (Fig. 1 and 2). The human pancreatic cancer cell line PANC-1 was RIP3 positive, but other pancreatic cancer lines not assayed such as MIA PaCa2 have reduced RIP3 expression (34). All the human glioblastoma cell lines in this experiment are RIP3 positive, but literature has shown that expression is variable in human glioma samples (27).

In addition to RIP3 and DAI protein expression, the functionality of the necroptosis pathway with death inducer TNFα and pan-caspase inhibitor zVAD was analyzed (Fig. 3, 4, 5, and 6). Since the TNFα pathway works by the RHIM domain-containing protein RIP1 and not DAI, a correlation between DAI expression and death was not expected and was not seen (Table 1 and 2). However, the requirement of interferon in murine cell lines for virus induced necroptosis, indicated a reliance on DAI for cell death as well (Fig. 7 and Table 2). However, a correlation between RIP3 expression and cell death was seen in most lines, murine and human (Table 1 and 2).

For most RIP3 positive cell lines, adding TNFα/zVAD (and LCL161 for human lines), resulting in a morphology change of cells shrinking, rounding up and uptaking the red propidium iodide dye (Fig. 3, 4, and 6). Necroptosis is an explosive death pathway that was seen with the morphology change in these cells. necroptosis. In addition, the timepoint of occurrence further supports the death pathway as necroptosis. Apoptosis takes longer to occur, often requiring 24 hours post-induction to see visible death. Lastly,

as RIP3 activity is required for necroptosis, adding RIP3 kinase inhibitor was able to rescue cells from TNFα/zVAD death (Fig. 5). These findings together support the idea that RIP3 positive cells are undergoing necroptosis and RIP3 negative cells are not.

The exceptions to this correlation were the PANC-1, U343, U251, and U87 cell lines which were RIP3 positive but not sensitive to TNFα/zVAD cell death (Fig. 1 and 4). For the PANC-1 pancreatic cancer cells, literature shows that they have RIP3 expression, matching these results (Fig.1), but have reduced expression of the effector protein MLKL, which is also necessary for necroptosis (34).

For the glioblastoma U251, U118 and U87, the RIP3 expression matches what is found in the literature (35, 36). While there was not a published figure supporting this, one paper claims that the U343 cells do not have detectable RIP3 expression, which contradicts the findings from this study (37). It is possible that some of the glioblastoma cell lines in our possession have undergone a change in MLKL expression and can no longer undergo necroptosis. Therefore, an important next step analysis would be to look at MLKL levels by western blot in all of these cancer cell lines.

While we were able to show necroptosis occurring from cytokine stimulation, the murine cells were also assayed for VACV stimulated DAI dependent necroptosis (Fig. 7). The RIP3 positive cell line underwent visible necroptosis as seen by dye exclusion and phosphorylation of MLKL when treated with TNFα/zVAD as well as IFN α and VACV-E3L mutants. Neither of the RIP3 negative cell lines uptook propidium iodide in response to the mutants and the K7M2 line did not phosphorylate or trimerize MLKL in response to any of the various stimuli tested (Fig. 8 and 9). Therefore, in the murine lines assayed, the VACV E3L mutants are able to induce necroptosis in cell lines that are

necroptosis/RIP3 positive but not in cell lines that are necroptosis/RIP3 negative (Table 2).

Looking at replication, one of the core requirements for oncolytic efficacy, single-step growth curves of wild-type VACV and the VACV E3L mutants were conducted. Only VACV-E3LΔ54N was used in the human cell lines (Fig. 10). For breast cancer and melanoma lines, the mutant was able to replicate in RIP3 negative lines but not in RIP3 positive lines. Previous mouse work in the RIP3 negative melanoma line MDA-MB-435S showed that VACV-E3LΔ54N reduced tumors locally at low doses and reduced adjacent tumors at high doses (33). Therefore, RIP3 expression, VACV E3L mutant replication, and oncolytic efficacy were correlated in SCID/bg human tumor models.

However, the data was less clear in the glioblastoma lines. Even though all the lines were RIP3 positive, the mutant was able to replicate in the three lines U251, U118, and U87 but was severely inhibited in the U343 cell line (Fig. 10). This could not be explained by the dye exclusion assay and possible MLKL explanation since the U118, not U343 cells showed propidium iodide uptake. For mouse work, VACV-E3LΔ54N did not reduce tumor volume of U118 or U251, despite successful viral replication (33). While this was hypothesized to be due to the vascular nature of the tumor and technical errors during implantation and infection, it is possible that there are also other mechanisms at play in glioblastoma that need to be characterized to understand the entire VACV-E3L mutant story in these cells.

In the mouse cell lines, replication of VACV-E3LΔ83N was looked at first. Both RIP3 negative cell lines allowed the replication of both VACV and the mutant. In the RIP3 positive cell line, VACV-E3LΔ83N replication was reduced. When VACV-

E3LΔ54N was added for comparison, it was clear that VACV-E3LΔ54N was more growth restricted in these cells than its counterpart (Fig. 11). This may be due in part to the fact that the Δ83N mutation produces a terminated E3 protein whereas Δ54N creates an unstable product, making it an even less pathogenic virus. For use as an oncolytic, the E3L mutants should be treated as separate entities as their growth kinetics are different and their oncolytic efficacy may vary as well.

Previous work has been done with B16 melanoma and VACV-E3LΔ54N tumor reduction. However, VACV-E3LΔ54N was chosen due to pathogenicity issues in SCID/bg mice. Therefore, an ongoing study is looking at the effect of VACV-E3LΔ83N in C57BL/6 mice with B16 melanoma.

Looking specifically at the melanoma, breast cancer, and osteosarcoma lines, a correlation between DAI/RIP3 expression and VACV-E3L mutant replication is evident. A SCID/bg mouse study comparing RIP3 positive and RIP3 negative primary human melanoma also indicates that there is a difference in VACV-E3LΔ54N oncolytic efficacy. However, this did not take into account intrinsic differences between cell lines. The other goal of this project was to create RIP3 matched pair of the same mouse cell line in order to further elucidate the role of RIP3 and to look at the effect of a fully intact immune system lacking in the SCID/bg mice. Therefore, we utilized molecular manipulation to modify RIP3 expression in the murine cell lines.

The first technique was to utilize the hypomethylating agent 5-AZA. One hypothesis as to why many cancer lines are deficient in RIP3 expression is that they are inducing hypermethylation and silencing the promoter in response to other changes, such as an increase of 2-HG (27). Literature indicates that some RIP3 negative cell lines can

expresses RIP3 and become sensitized to TNFα/zVAD necroptosis after 5-AZA treatment, which would support this hypothesis (26). The L929 results matched previous literature, with a decrease in TNFα/zVAD sensitivity (Fig. 12) (26). Since 5-AZA is a non-specific hypomethylating agent, it is possible that it is upregulating another unknown inhibitor of cell death. However, while the literature showed successful upregulation of RIP3 in B16 cells, this experiment could not be repeated in this study due to cell sensitivity. Instead, the K7M2 osteosarcoma line was characterized.

Unlike the B16 in literature, the K7M2 cells did not increase RIP3 expression or become more sensitive to TNFα/zVAD cell death (Fig. 12). This implies that RIP3 loss in the K7M2 cells is not as a result of methylation. Instead, this loss may be a genetic deletion rather than an epigenetic change. Further work on this may involve testing other RIP3 negative cell lines including the 4T1 mouse breast cancer. Conversely, future work should also involve testing hypermethylating agents such as 2-HG to see if protein expression in RIP3 positive lines like E0771 can be abrogated. While this technique may not help with model building, the human lines should also be analyzed with these reagents to further explore the methylation hypothesis. An advantage of confirming the link between methylation and RIP3 expression is that already established biomarkers such as IDH that result in hypermethylation could be used as surrogate biomarkers for RIP3 expression in the clinic (27). With a biomarker for which tumors are more likely to respond to the VACV E3L mutant therapy, clinicians will be able to select patients who would gain the most from this therapy and increase the chance of the oncolytic being approved for licensure.

Another avenue for more stable RIP3 manipulation is the CRISPR-Cas9 system. Originally isolated from Staphylococcus bacteria, this method was optimized to edit mammalian cells. The Cas9 enzyme utilizes a guide RNA that targets a specific region of the genome and induces double-stranded breaks and can cause a non-functional target gene. While Cas9 and guide RNAs can be transiently transfected for short term knockout studies, the aim of this project was to produce stable knockout cell lines that can be used in mouse tumor studies. Therefore, Cas9 and a RIP3 targeting guide RNA were stably transduced in E0771 cells using lentiviruses. The Cas9 was delivered with a commercial lentivirus and Cas9 expression was confirmed by immunocytochemistry (Fig. 13). However, not all cells were Cas9 positive and no selection was done before moving to the next step, which may reduce the percentage of successful knockout cells in later steps. The guide RNA for knocking out mouse RIP3 was ordered as a commercial, validated lentiviral transfer plasmid called pLentiguide-Puro that utilized a second-generation packaging system. This lentivirus was able to confer puromycin resistance and continued selection with puromycin seems to indicate loss of TNFα/zVAD sensitivity in some cells. (Fig 14-15). Future work will be to further select the cells using colony selection and western blot confirmation of RIP3 negativity. Once this is done, this cell line can be implanted in mice alongside RIP3 positive E0771 cells and oncolytic efficacy can be compared.

With the rising popularity of more precise cancer therapies such as immunotherapy and its corollary field of virotherapy, this study provided insight into a new therapy. In addition, with the frequency of tumors that have evolved malfunctions in the antiviral cell death pathway necroptosis and the reliance of many chemotherapeutics

on necroptotic functionality this virotherapy strategy fills a gap in treatment options. Even as a combination therapy with chemotherapy or immunotherapy, the VACV E3L mutants may even help provide a better clinical outcome in patients in the future. Therefore, this study provides a valuable addition to the field of oncology.

REFERENCES

1. Kohlhapp FJ, Kaufman HL. 2016. Molecular Pathways: Mechanism of Action for Talimogene Laherparepvec, a New Oncolytic Virus Immunotherapy. Clinical Cancer Research 22:1048-1054.
2. Seymour LW, Fisher KD. 2016. Oncolytic viruses: finally delivering. British Journal of Cancer 114:357-361.
3. Gorgas WC. 1902. The Method of Transmission of Yellow Fever from Man to Man. Public health papers and reports 28:238.
4. Dock G. 1904. THE INFLUENCE OF COMPLICATING DISEASES UPON LEUKÆMIA.*. The American Journal of the Medical Sciences 127:563-592.
5. Bierman HR, Crile DM, Dod KS, Kelly KH, Petrakis NI, White LP, Shimkin MB. 1953. Remissions in leukemia of childhood following acute infectious disease. Staphylococcus and streptococcus, varicella, and feline panleukopenias. Cancer 6:591-605.
6. Hoster HA, Zanes RP, Haam EV. 1949. Studies in Hodgkin's Syndrome IX. The Association of “Viral” Hepatitis and Hodgkin's Disease (A Preliminary Report). Cancer Research 9:473-480.
7. Southam CM, Moore AE. 1952. Clinical studies of viruses as antineoplastic agents, with particular reference to egypt 101 virus. Cancer 5:1025-1034.
8. Martuza R, Malick A. 1991. Experimental Therapy of Human Glioma by Means of a Genetically Engineered Virus Mutant. Science 252:854.
9. Ganly I, Kirn D, Eckhardt G, Rodriguez GI, Soutar DS, Otto R, Robertson AG, Park O, Gulley ML, Heise C, Von Hoff DD, Kaye SB, Eckhardt SG. 2000. A phase I study of Onyx-015, an E1B attenuated adenovirus, administered intratumorally to patients with recurrent head and neck cancer. Clinical cancer research : an official journal of the American Association for Cancer Research 6:798-806.
10. Russell L, Peng KW. 2018. The emerging role of oncolytic virus therapy against cancer. Chinese Clinical Oncology 7:13.
11. Guo ZS, Lu BF, Guo ZB, Giehl E, Feist M, Dai EY, Liu WL, Storkus WJ, He YK, Liu ZQ, Bartlett DL. 2019. Vaccinia virus-mediated cancer immunotherapy: cancer vaccines and oncolytics. Journal for Immunotherapy of Cancer 7:21.
12. Distefano AD, Buzdar AU. 1979. VIRAL-INDUCED REMISSION IN CHRONIC LYMPHOCYTIC-LEUKEMIA. Archives of Internal Medicine 139:946-946.
13. Arakawa S, Hamami G, Umezu K, Kamidono S, Ishigami J. 1987. CLINICAL-TRIAL OF ATTENUATED VACCINIA VIRUS AS STRAIN IN THE TREATMENT OF ADVANCED ADENOCARCINOMA - REPORT ON 2 CASES. Journal of Cancer Research and Clinical Oncology 113:95-98.

14. Kawa A, Arakawa S. 1987. THE EFFECT OF ATTENUATED VACCINIA VIRUS AS STRAIN ON MULTIPLE-MYELOMA - A CASE-REPORT. Japanese Journal of Experimental Medicine 57:79-81.

15. Parato KA, Breitbach CJ, Le Boeuf F, Wang JH, Storbeck C, Ilkow C, Diallo JS, Falls T, Burns J, Garcia V, Kanji F, Evgin L, Hu K, Paradis F, Knowles S, Hwang TH, Vanderhyden BC, Auer R, Kirn DH, Bell JC. 2012. The Oncolytic Poxvirus JX-594 Selectively Replicates in and Destroys Cancer Cells Driven by Genetic Pathways Commonly Activated in Cancers. Molecular Therapy 20:749-758.

16. Colamonici OR, Domanski P, Sweitzer SM, Larner A, Buller RML. 1995. VACCINIA VIRUS B18R GENE ENCODES A TYPE-I INTERFERON-BINDING PROTEIN THAT BLOCKS INTERFERON-ALPHA TRANSMEMBRANE SIGNALING. Journal of Biological Chemistry 270:15974-15978.

17. White SD, Jacobs BL. 2012. The Amino Terminus of the Vaccinia Virus E3 Protein Is Necessary To Inhibit the Interferon Response. Journal of Virology 86:5895-5904.

18. Mitnik C. 2004. Poxvirus interferon -resistance genes: Their evolutionary past and role in anti-cancer therapy. ProQuest Dissertations Publishing.

19. Cho Y, Challa S, Moquin D, Genga R, Ray TD, Guildford M, Chan FKM. 2009. Phosphorylation-Driven Assembly of the RIP1-RIP3 Complex Regulates Programmed Necrosis and Virus-Induced Inflammation. Cell 137:1112-1123.

20. Feng SS, Yang YH, Mei Y, Ma L, Zhu DE, Hoti N, Castanares M, Wu M. 2007. Cleavage of RIP3 inactivates its caspase-independent apoptosis pathway by removal of kinase domain. Cellular Signalling 19:2056-2067.

21. Zhang DW, Shao J, Lin J, Zhang N, Lu BJ, Lin SC, Dong MQ, Han JH. 2009. RIP3, an Energy Metabolism Regulator That Switches TNF-Induced Cell Death from Apoptosis to Necrosis. Science 325:332-336.

22. He S, Wang L, Miao L, Wang T, Du F, Zhao L, Wang X. 2009. Receptor Interacting Protein Kinase-3 Determines Cellular Necrotic Response to TNF-α. Cell 137:1100-1111.

23. Vandenabeele P, Galluzzi L, Vanden Berghe T, Kroemer G. 2010. Molecular mechanisms of necroptosis: an ordered cellular explosion. Nature Reviews Molecular Cell Biology 11:700-714.

24. Koehler H, Cotsmire S, Langland J, Kibler KV, Kalman D, Upton JW, Mocarski ES, Jacobs BL. 2017. Inhibition of DAI-dependent necroptosis by the Z-DNA binding domain of the vaccinia virus innate immune evasion protein, E3. Proceedings of the National Academy of Sciences of the United States of America 114:11506-11511.

25. Imre G. 2020. The involvement of regulated cell death forms in modulating the bacterial and viral pathogenesis.

26. Koo GB, Morgan MJ, Lee DG, Kim WJ, Yoon JH, Koo JS, Kim SI, Kim SJ, Son MK, Hong SS, Levy JMM, Pollyea DA, Jordan CT, Yan P, Frankhouser D, Nicolet D, Maharry K, Marcucci G, Choi KS, Cho H, Thorburn A, Kim YS. 2015. Methylation-dependent loss of RIP3 expression in cancer represses programmed necrosis in response to chemotherapeutics. Cell Research 25:707-725.

27. Yang ZT, Jiang B, Wang Y, Ni HX, Zhang J, Xia JM, Shi MG, Hung LM, Ruan JS, Mak TW, Li QX, Han JH. 2017. 2-HG Inhibits Necroptosis by Stimulating DNMT1-Dependent Hypermethylation of the RIP3 Promoter. Cell Reports 19:1846-1857.

28. Dull T, Zufferey R, Kelly M, Mandel RJ, Nguyen M, Trono D, Naldini L. 1998. A third-generation lentivirus vector with a conditional packaging system. Journal of Virology 72:8463-8471.

29. Sanjana NE, Shalem O, Zhang F. 2014. Improved vectors and genome-wide libraries for CRISPR screening. Nature Methods 11:783-784.

30. Holliday DL, Speirs V. 2011. Choosing the right cell line for breast cancer research. Breast Cancer Research 13:7.

31. Lu C, Zhou L-y, Xu H-j, Chen X-y, Tong Z-s, Liu X-d, Jia Y-s, Chen Y. 2014. RIP3 overexpression sensitizes human breast cancer cells to parthenolide in vitro via intracellular ROS accumulation. Acta Pharmacologica Sinica 35:929-936.

32. Trainor KL. 2008. The use of vaccinia virus E3L amino-terminal mutants in viral oncolysis and characterization in the murine JC cell lineThesis (Ph. D.)--Arizona State University, 2008.

33. Arndt W. 2010. Characterization of the E3L amino-terminus in poxvirus replication and tumor regression. ProQuest Dissertations Publishing.

34. Ando Y, Ohuchida K, Otsubo Y, Sagara A, Kibe S, Takesue S, Nakayama M, Shindo K, Moriyama T, Nakata K, Ohtsuka T, Mizumoto K, Nakamura M. 2019. Necroptosis in Pancreatic Cancer Promotes Cancer Cell Migration and Invasion by Release of CXCL5. Pancreas 48:1403-1404.

35. Lu B, Gong X, Wang Z-q, Ding Y, Wang C, Luo T-f, Piao M-h, Meng F-k, Chi G-f, Luo Y-n, Ge P-f. 2017. Shikonin induces glioma cell necroptosis in vitro by ROS overproduction and promoting RIP1/RIP3 necrosome formation. Acta Pharmacologica Sinica 38:1543-1553.

36. Melo-Lima S, Celeste Lopes M, Mollinedo F. 2014. Necroptosis is associated with low procaspase-8 and active RIPK1 and -3 in human glioma cells. Oncoscience 1:649-664.

37. Meyer N, Zielke S, Michaelis JB, Linder B, Warnsmann V, Rakel S, Osiewacz HD, Fulda S, Mittelbronn M, Muench C, Behrends C, Koegel D. 2018. AT 101 induces early mitochondrial dysfunction and HMOX1 (heme oxygenase 1) to trigger mitophagic cell death in glioma cells. Autophagy 14:1693-1709.

59